

## **General Disclaimer**

### **One or more of the Following Statements may affect this Document**

- This document has been reproduced from the best copy furnished by the organizational source. It is being released in the interest of making available as much information as possible.
- This document may contain data, which exceeds the sheet parameters. It was furnished in this condition by the organizational source and is the best copy available.
- This document may contain tone-on-tone or color graphs, charts and/or pictures, which have been reproduced in black and white.
- This document is paginated as submitted by the original source.
- Portions of this document are not fully legible due to the historical nature of some of the material. However, it is the best reproduction available from the original submission.

**NASA TECHNICAL  
MEMORANDUM**

NASA TM X-73568

NASA TM X-73568

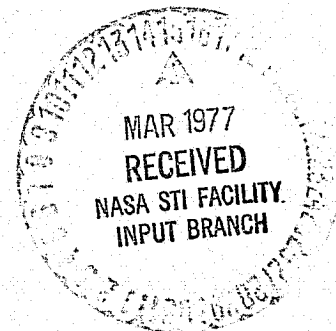
(NASA-TM-X-73568) EFFECT OF ENDWALL COOLING  
ON SECONDARY FLOWS IN TURBINE STATOR VANES  
(NASA) 29 p HC A03/MF A01 CSCL 21E

N77-18159

G3/07 Unclass  
17207

**EFFECT OF ENDWALL COOLING ON SECONDARY  
FLOWS IN TURBINE STATOR VANES**

by Louis J. Goldman and Kerry L. McLallin  
Lewis Research Center  
Cleveland, Ohio 44135



TECHNICAL PAPER to be presented at the  
AGARD Forty-ninth Propulsion and Energetics Panel Conference  
The Hague, Netherlands, March 28-April 4, 1977

## EFFECT OF ENDWALL COOLING ON SECONDARY FLOWS IN TURBINE STATOR VANES

Louis J. Goldman and Kerry L. McLallin

National Aeronautics and Space Administration  
Lewis Research Center  
Cleveland, Ohio, 44135

## SUMMARY

An experimental investigation was performed to determine the effect of endwall cooling on the secondary flow behavior and the aerodynamic performance of a core-turbine stator vane. The investigation was conducted in a cold-air, full-annular cascade, where three-dimensional effects could be obtained. Two endwall cooling configurations were tested. In the first configuration, the cooling holes were oriented so that the coolant was injected in line with the inviscid streamline direction. In the second configuration, the coolant was injected at an angle of  $15^\circ$  to the inviscid streamline direction and oriented toward the vane pressure surface. In both cases the stator vanes were solid and uncooled so that the effect of endwall cooling could be obtained directly.

Total-pressure surveys were taken downstream of the stator vanes over a range of cooling flows at the design, mean-radius, critical velocity ratio of 0.778. Changes in the total-pressure contours downstream of the vanes were used to obtain the effect of endwall cooling on the secondary flows in the stator. Comparisons are made between the two cooled-endwall configurations and with the results obtained previously for solid (uncooled) endwalls. The results presented in this paper are the first part of a comprehensive program of endwall cooling studies currently in progress at NASA.

## SYMBOLS

$C_p$	specific heat at constant pressure, J/kg-K (Btu/lbm- $^\circ$ R)
$E$	energy parameter, eq. (4)
$g$	force-mass conversion constant, 32.174 lbf-ft/lbf-sec <sup>2</sup>
$J$	mechanical equivalent of heat, 778.0 ft-lbf/Btu
$J_z$	axial momentum parameter, eq. (2)
$J_\theta$	tangential momentum parameter, eq. (3)
$M$	Mach number
$\bar{m}$	mass flow parameter at radius $r$ , eq. (1)
$\bar{\bar{m}}$	total mass flow per passage, kg/sec (lbfm/sec)
$p$	pressure, N/m <sup>2</sup> (lbf/ft <sup>2</sup> )
$\bar{p}$	circumferentially mixed pressure at radius $r$ , N/m <sup>2</sup> (lbf/ft <sup>2</sup> )
$p_c$	inlet pressure of coolant, N/m <sup>2</sup> (lbf/ft <sup>2</sup> )
$p_0$	inlet pressure of primary flow, N/m <sup>2</sup> (lbf/ft <sup>2</sup> )
$R$	gas constant, J/kg-K (ft-lbf/lbm- $^\circ$ R)
$r$	radial direction, m (ft)
$T$	temperature, K ( $^\circ$ R)
$T_c$	inlet temperature of coolant, K ( $^\circ$ R)
$T_0$	inlet temperature of primary flow, K ( $^\circ$ R)
$V$	velocity, m/sec (ft/sec)
$y$	mass flow fraction
$z$	axial direction, m (ft)
$\alpha$	flow angle measured from axial direction, deg
$\gamma$	ratio of specific heats
$\bar{\eta}$	overall efficiency based on kinetic energy

ORIGINAL PAGE IS  
OF POOR QUALITY

$\theta$  vane angular spacing, deg  
 $\theta$  circumferential direction, deg  
 $\rho$  density,  $\text{kg/m}^3$  ( $\text{lbm/ft}^3$ )

## Subscripts:

c coolant flow  
 cr flow condition at Mach 1  
 h hub  
 i survey position closest to inner (hub) wall  
 id ideal or isentropic process  
 L lower or pressure surface  
 o survey position closest to outer (tip) wall  
 p primary flow  
 s solid (uncooled)  
 T thermodynamic  
 t tip  
 U upper or suction surface  
 z axial direction  
 $\theta$  tangential direction  
 0 station at inlet plane of cascade bellmouth, fig. 2  
 1 station at vane inlet, fig. 2  
 2 station at vane trailing edge, fig. 2  
 3 station downstream of vane trailing edge where survey measurements were taken, fig. 2  
 3M station far downstream of vane trailing edge where flow was assumed to be circumferentially mixed (uniform), fig. 2

## Superscript:

' total-state condition

## INTRODUCTION

Experimental investigations are being conducted at the NASA Lewis Research Center (refs. 1 to 3) and under contract (ref. 4) to obtain the aerodynamic performance of air-cooled blading and endwalls for high-temperature, core-engine turbines. As part of this effort, the performance of a solid (uncooled) version of the core stator has been determined in a full-annular cascade (ref. 3). These results form the basis of comparison for the cooled versions of the core stator and endwalls. Downstream of the solid vanes and endwalls, two vortex cores of high loss concentration are located at the corners formed by the endwalls and the vane suction surface (ref. 3). Because of the low aspect ratio of these vanes (the ratio of vane height to vane axial chord is 1.0), these losses were expected and were identified with the secondary flows present in the stator. The secondary flow loss for the solid vanes and endwalls was estimated (ref. 3) to be a significant portion (about 28 percent) of the total loss. For cooled stators, one possible method of reducing these losses is to use the injected endwall coolant to modify the secondary flows in the stator vanes.

A test program was, therefore, undertaken to study the effect of endwall cooling on these secondary flows. Parameters to be investigated in the endwall cooling program include cooling hole location, cooling hole size, blowing rate, and coolant injection angle. The first part of this study, and the subject of this paper, is the effect of endwall coolant injection angle on these secondary flows and on the vane aerodynamic performance.

Two similar endwall cooling configurations were experimentally studied. In the first configuration, three rows of cooling holes were oriented so that the endwall coolant was injected in line with the inviscid streamline direction. In the second configuration, the coolant was injected at an angle of  $15^\circ$  to the inviscid streamline direc-

tion and oriented toward the vane pressure surface. In both cooled-endwall configurations, the coolant was injected at an angle of  $15^\circ$  to the endwall surface and the stator vanes were solid (uncooled), so that the effect of endwall cooling could be obtained directly. The coolant was injected at  $15^\circ$  to the inviscid streamline direction in the second configuration in an attempt to impede the crossflows that occur in the endwall boundary layers and thereby to decrease the secondary flow losses. In addition, flow visualization studies on flat plates (ref. 5) have shown that coolant injected at an angle to the streamwise flow direction tends to prevent the cooling film from separating from the surface even at high blowing rates. It might be possible, therefore, to reduce the secondary flow losses and by the same means increase the film cooling effectiveness.

The cooled-endwall investigation was conducted at the vane design, mean-radius, aftermixed, critical velocity ratio of 0.778. Annular total-pressure surveys were taken downstream of the vanes over a range of coolant to primary inlet total-pressure ratios from 1.0 to 2.0. This corresponds to coolant flow rates from 0.9 to 3.1 percent of the primary flow. All tests were conducted with primary air at ambient conditions at the cascade inlet and with a primary to coolant total-temperature ratio of 1.0. It was thought that a valid comparison of the two cooled-endwall configurations could be made at this temperature ratio. In addition, the cold-test data can be used to predict the performance at actual engine temperature ratios by the method described in reference 6.

This paper describes the two endwall cooling configurations tested and the results obtained. Total-pressure contours downstream of the vanes are presented for selected coolant to primary total-pressure ratios. Changes in these total-pressure patterns are used to obtain the effect of endwall cooling on the secondary flow in the stator. How the vane aftermixed total pressure varies with radial position is shown for these coolant to primary total-pressure ratios. The percent change in aftermixed efficiency (from the solid endwalls) per percent coolant is also shown over the range of total-pressure ratios tested. The cooled-endwall results are compared, where applicable, with the results obtained for the solid (uncooled) endwalls. Comparisons are also made between the two endwall configurations tested. This paper also includes a description of future work planned in the endwall cooling program.

## APPARATUS, INSTRUMENTATION, AND PROCEDURE

### Cascade Facility

The full-annular cascade facility consists primarily of an inlet section, a test section, and an exit section. The actual facility and a cross-sectional view of the facility are shown in figures 1 and 2, respectively. In operation, primary or mainstream air (at ambient conditions) is drawn from the test cell through the inlet section, the blading, and the exit section and then is exhausted through the laboratory exhaust system. Cooling air at room temperature and  $27.58 \text{ N/cm}^2$  (40 psig) is supplied by the laboratory combustion air system and is routed to the individual coolant circuits as shown in figures 1 and 2. For this investigation, only the hub and tip endwall cooling air was used since the vanes were solid (uncooled).

Inlet section. - The inlet, consisting of a bellmouth and a short straight section, was designed to accelerate the flow to uniform axial flow at the vane inlet. The bellmouth was designed to provide a smooth transition to the straight section and to minimize the boundary layer growth.

Test section. - The test section consists of a section of five vanes that are part of the full-annular ring of 36 vanes. As seen in figure 2, the vanes pass through two hollow vane rings (endwalls). This allows cooling air to be independently supplied to both the vanes and the endwalls. For the endwall cooling investigation reported herein, all the vanes were solid (uncooled). Only the four endwall passages between the five test vanes were cooled.

The stator vane geometry (same aerodynamic profile as in refs. 1 to 4) is shown in figure 3. The untwisted vanes, of constant profile from hub to tip, have a height of 3.81 centimeters (1.50 in.), an axial chord of 3.823 centimeters (1.505 in.), and a trailing-edge radius of 0.089 centimeter (0.035 in.). The vane aspect ratio and solidity at the mean section are 1.00 and 0.93, respectively, based on axial chord. The stator hub-to-tip radius ratio is 0.85 and the mean radius is 23.50 centimeters (9.25 in.).

Exit section. - The exit section consists primarily of a diffusing section and a flow straightening section (fig. 2). The diffusing section decelerates the flow downstream of the 3M station. The flow straightening section turns the swirling flow back to the axial direction prior to its entering the laboratory exhaust system. The straightener consists of a bundle of short tubes with centerlines parallel to the cascade axis (fig. 2).

### Endwall Cooling Configurations

Two similar endwall cooling configurations were tested. A schematic representation of the configurations is shown in figure 4 for the hub endwall. In the first configuration, three rows of cooling holes were oriented so that the endwall coolant was injected in line with the inviscid streamline direction. In the second configuration, the coolant (within the vane passage) was injected at an angle of  $15^\circ$  to the inviscid streamline di-

rection and oriented toward the vane pressure surface. This was done in an attempt to impede the crossflows that occur in the endwall boundary layers and thereby to decrease the secondary flow losses.

The endwall cooling geometry and coordinates are presented in figure 5 and in table I. The in-line coolant injection configuration was designed for NASA under contract (ref. 4). This design had a row of cooling holes upstream of the vane leading edge, on both the hub and tip endwalls, which could not be fabricated in our hollow vane rings. In addition, as noted in table I, a number of cooling holes (primarily in the first row of holes) on the hub endwall could not be fabricated. This was caused by the shallow coolant injection angle ( $15^\circ$  to the endwall surface) and the excessive hub endwall thickness that occurred during fabrication. To make comparison of the two configurations easier, the holes that could not be machined in the second configuration were filled with epoxy in the first configuration. In this way both configurations had the same number (and location) of open cooling holes (fig. 4). The row of cooling holes downstream of the vane trailing edge, on the tip endwall, were 0.038 centimeter (0.015 in.) in diameter and were aligned near the design flow angle for both configurations. All other cooling holes were 0.051 centimeter (0.020 in.) diameter. The actual hub and tip hollow vane rings for the first configuration (with all cooling holes open) are shown in figure 6.

#### Instrumentation

Instrumentation was provided to measure inlet total temperature and pressure, wall static pressures upstream and downstream of the test section, survey data of vane exit total pressure, and coolant supply conditions. All pressures were measured with calibrated strain-gage transducers, and all temperatures were measured with copper-constantan thermocouples. Figure 2 shows the station nomenclature used for the instrumentation.

Inlet total conditions. - The total temperature of the primary air was measured by four thermocouples located  $90^\circ$  apart circumferentially at the bellmouth inlet (station 0). The ambient pressure was measured by a transducer located near the cascade inlet. Prior to the subject investigation, boundary layer measurements of total pressure were made near the vane inlet (station 1).

Wall static pressures. - Static pressures were measured at various locations in the cascade by 0.051-centimeter (0.020-in.) diameter pressure taps located on both the hub and tip walls. At a distance of one axial chord length upstream of the vane inlet (station 1), four taps were located  $90^\circ$  apart circumferentially. These taps were used primarily to check the uniformity of the flow entering the vanes. At the vane exit survey plane (station 3), eight taps (on both the hub and tip endwalls) spanned the test section and were spaced circumferentially as shown in figure 7. These pressures were used to estimate the variation of static pressure with radius for use in the aerodynamic performance calculations. Two static taps (hub and tip wall) were also located 10.2 centimeters (4.0 in.) axially downstream of the vanes, where the flow would probably be mixed to relatively uniform conditions (station 3M). This hub static pressure was used to set the primary airflow conditions in the cascade.

Survey probe. - Vane aerodynamic performance data were obtained with the two-element, total-pressure probe shown in figure 8. This type of fixed-position probe allows survey data to be taken near both the hub and tip walls. The hub element (fig. 8) was used for measurements in the region that extended from near the hub wall up to a radial position of 75 percent of the vane span. The tip element was used in the remaining tip region. The survey plane (station 3, fig. 7) was 1.3 centimeters (0.5 in.) axially downstream of the vane trailing edge with the probe positioned at a fixed angle of  $67^\circ$  from the axial direction (design flow angle). Survey data were taken over three vane wakes to check for periodicity.

The probe elements were made of stainless-steel tubing having an outside diameter of 0.051 centimeter (0.020 in.) and an inside diameter of 0.038 centimeter (0.015 in.). The total-pressure tubes had inside bevels of  $30^\circ$ , which reduce the sensitivity of the total-pressure measurement to flow angle variations (ref. 7). The loss in total pressure was measured with a differential pressure transducer referenced to atmospheric pressure.

Coolant flow conditions. - The coolant flow rate was measured with calibrated venturi meters of various sizes. The venturi meters and runs conformed to ASME specifications and were calibrated before installation. The endwall coolant total pressures and temperatures were assumed to be equal to the static measurements made before the coolant entered the hollow vane rings (fig. 1). Errors of less than 1 percent resulted from this assumption because of the small coolant flow velocities (Mach numbers less than 0.1) in the supply tubing.

#### Test Procedure

To operate the full-annular cascade facility, atmospheric air from the test cell was drawn through the cascade and exhausted into the laboratory exhaust system. The primary airflow conditions were set by controlling the pressure ratio across the stator vanes with a throttle valve located in the exhaust system. The hub static-pressure tap located at station 3M downstream of the vane exit was used to set this pressure ratio.

Cooling air, at room temperature and  $27.58 \text{ N/cm}^2$  (40 psig), was supplied by the

laboratory combustion air system. The desired coolant flow rate was obtained by setting the pressure upstream of the venturi with a pressure regulator and controlling the venturi pressure ratio with a throttle valve located downstream of the venturi run.

The two endwall cooling configurations were tested at an exit static- to inlet total-pressure ratio that corresponded to the design, mean-radius, ideal, aftermixed, critical velocity ratio of 0.778. Nominal coolant to primary inlet total-pressure ratios  $p_c'/p_0'$  of 1.0, 1.2, 1.4, 1.6, 1.8, and 2.0 were set by varying the coolant flow rates from 0.9 to 3.1 percent of the primary flow. For any given test, this pressure ratio was maintained the same for the hub and tip endwall coolants, as this would correspond to usual engine operation.

At a given flow condition, probe survey data were obtained at a number of different radii (typically 23) from hub to tip. At any fixed radius, the probe moved circumferentially in a continuous manner behind the middle three vanes of the five-vane test section, with survey data being recorded at 0.08-degree increments (fig. 7). The vane spacing  $\theta$  of  $10^\circ$  results in about 125 measurement points per vane. The output signals of the thermocouples and pressure transducers were digitized for all the data and recorded on magnetic tape for permanent record.

#### Data Reduction

The cooled aerodynamic performance presented herein was calculated from the measurement of the survey probe total pressure, the wall static pressures at the survey plane (station 3), and the probe position. Data from the middle test vane (of the three vanes that were surveyed) were used in these calculations. Since only the vane exit total pressure was measured for these tests, the following assumptions were made for data reduction purposes:

- (1) The static pressure at the survey plane (station 3) is constant circumferentially and varies linearly with radius. The hub and tip wall static pressures at station 3 were used for this interpolation.
- (2) The flow angle at the survey plane is constant circumferentially and radially. The design value of  $67^\circ$  was used for the performance data presented herein.
- (3) The total temperature at the survey plane is constant and equal to the total temperature at the bellmouth inlet (station 0).

The calculated vane performance was compared in reference 3 with data obtained from a total-pressure probe (similar to the one used in this paper) by using the previous assumptions and from a combination probe (measuring total pressure, static pressure, and flow angle). Excellent agreement was found in the results obtained for the two probe types. The main advantage of the probe type used herein is that measurements close to both walls can be made without changing probes.

The calculation of vane performance is based on the determination of a hypothetical state where it is assumed that the flow has mixed to a circumferentially uniform condition. The application of the conservation equations to an annular-sector control volume to obtain this aftermixed state, at each radius, has been described fully in reference 8 and is summarized in the appendix. The aftermixed vane efficiency, based on kinetic energy, is used herein because it is theoretically independent of the location of the survey measurement plane. In addition, the aftermixed state represents the "average" conditions seen by the rotor. Note that the aftermixed efficiency contains not only the solid boundary friction losses but also the mixing losses.

#### RESULTS AND DISCUSSION

Presented in this section are the experimentally determined, survey plane, total-pressure contours, the variation of aftermixed total pressure with radius, and the overall vane aerodynamic performance. Comparisons are made between the two cooled-endwall configurations and the solid endwall. The solid-endwall performance, which serves as a basis of comparison for the cooled endwalls, is discussed first.

##### Solid (Uncooled) Endwalls

For test program flexibility, two physically distinct sets of hollow vane rings (endwalls) and vanes were used for the endwall cooling investigation reported herein. With this arrangement, one configuration could be tested while the other configuration was being fabricated. Having two distinct endwall sets did, however, lead to some difficulties as it was observed that there were some small geometric differences in the two sets. Because of this the performance of the solid (uncooled) version of each endwall set had to be experimentally determined. These results then formed the basis of comparison for the corresponding cooled version of each vane and endwall set.

The survey plane total-pressure  $p_3'$  characteristics for the solid (uncooled) endwall sets are compared in figure 9. The higher loss regions in figure 9 (i.e.,  $p_3'/p_0' \leq 0.93$ ) have been crosshatched for easier comparison of the two configurations. Two cores of high loss, centered at approximately 10 and 80 percent of vane height, are located on

the suction side of the trailing-edge projection, for each endwall set. As discussed in reference 3, these loss regions are associated with the movement of secondary flows within the endwall boundary layers from the pressure surface to the suction surface in the vane passage. This flow is then turned away from the endwalls and rolls up to form passage vortices in the corners formed by the endwalls and the vane suction surface. Close inspection of figure 9 shows that the losses are somewhat higher and extend further into the mean section (fig. 9) for the endwall set that was subsequently used for the in-line coolant ejection tests. This can be more easily seen in the next figure.

Another comparison of the two solid endwall sets is shown in figure 10, where the aftermixed to inlet total-pressure ratio  $\bar{p}_{3M}/p_0'$  is presented as a function of vane height. The wall static to inlet total-pressure ratios (at the survey plane) were 0.65 and 0.73 for the hub and tip walls, respectively. The solid endwall set used for the in-line coolant injection tests again shows higher losses, particularly, in the vortex core regions. The overall aftermixed efficiency  $\bar{\eta}_{3M,s}$  for this endwall set was 96.17 percent, while that for the solid endwall set used for the coolant injected at  $15^\circ$  to the in-line direction was 96.53 percent.

Also shown in figure 10 is the vane inlet to bellmouth inlet total-pressure ratio  $p_1/p_0'$  as a function of vane height, which was determined for the in-line configuration only. The inlet boundary layer probe was removed prior to obtaining the vane exit survey data to prevent any interference effects. The calculated displacement and momentum thickness per percentage of vane height were 1.51 and 0.56, respectively. Because of the small difference between  $p_0'$  and  $p_1$  and the negligible effect on the results, the bellmouth total pressure  $p_0'$  has been used as a basis of comparison in all figures and calculations.

#### Endwall Coolant Flow Characteristics

The coolant flow characteristics for the two endwall configurations are shown in figure 11. The hub, tip, and total endwall coolant flows as percentages of primary flow are shown as functions of coolant to primary inlet total-pressure ratio  $p_c'/p_0'$ . The coolant flow for the tip endwall is about twice that for the hub endwall because of the larger number of coolant holes on the tip endwall. The in-line coolant injection configuration has a 10 to 15 percent higher coolant flow than the  $15^\circ$  to in-line coolant injection configuration. Since the number of coolant holes were the same in each configuration, this flow difference is caused by hole size differences (due to fabrication tolerances) and possibly to different coolant flow discharge coefficients. At a pressure ratio  $p_c'/p_0'$  of 1.0 (which is representative of first-stage engine conditions), the total endwall coolant flow fractions  $y_c$  are 1.0 and 0.9 for the in-line and the  $15^\circ$  to in-line coolant injection configurations, respectively.

#### Total-Pressure Contours and Secondary Flows

Contours of vane exit to inlet total-pressure ratio  $p_3'/p_0'$  are shown in figures 12 and 13 for the two cooled-endwall configurations at selected coolant to primary total-pressure ratios  $p_c'/p_0'$ . The survey probe total-pressure data were used to generate these computer contour plots. Also shown again, for ease of comparison, are the results obtained for the solid (uncooled) version of each endwall set. The higher loss regions in figures 12 and 13 (i.e.,  $p_3'/p_0' \leq 0.93$ ) have again been crosshatched for comparison purposes.

At a total-pressure ratio  $p_c'/p_0'$  of 1.0, both configurations show larger vortex core losses (more area) than do the corresponding solid (uncooled) endwalls. This indicates, as might be expected, that the low-momentum endwall coolant has migrated to the passage vortex regions. The in-line coolant injection configuration has somewhat larger losses than the  $15^\circ$  to in-line coolant injection configuration. This is shown by the appearance of higher loss contours (N and M) in the hub and tip regions of the in-line coolant injection configuration where none existed in the solid configuration. In addition, comparing loss contours J indicates that more tip endwall coolant has migrated radially down the trailing-edge region for the in-line coolant injection configuration. From these results it is concluded that the coolant injected at an angle of  $15^\circ$  to the in-line direction has, to some extent, been successful in impeding the secondary flows that occur in cooled-endwall stators. Further improvements may also be possible if the coolant is injected at angles greater than  $15^\circ$  to the in-line direction.

At total-pressure ratios  $p_c'/p_0'$  greater than 1.0, the total-pressure losses decrease for both cooled-endwall configurations. Again the improvements are larger for the  $15^\circ$  to in-line coolant injection configuration. At a total-pressure ratio  $p_c'/p_0'$  of 1.8, comparing the total-pressure contours with the trailing-edge projection shows that the underturning of the flow that occurs at lower total-pressure ratios  $p_c'/p_0'$  and for the solid endwall has to a large extent been eliminated. This is due to the increased momentum of the endwall coolant. It is particularly striking in the tip region and is probably enhanced by the row of coolant holes downstream of the vane trailing edge (fig. 5). The improvement in the flow conditions to the rotor blades would be expected to increase the turbine performance by decreasing the primary airflow blockage and rotor incidence losses.



### Aftermixed Total-Pressure Characteristics

The variation of aftermixed to inlet total-pressure ratio  $P_{3M}/P_0'$  with vane height is shown in figures 14 and 15 for the two cooled-endwall configurations at selected coolant to primary total-pressure ratios  $p_c/p_0'$ . The corresponding solid-endwall cases are also shown in the figures for comparison with the cooled-endwall results. At a total-pressure ratio  $p_c/p_0'$  of 1.0, there is an increase in the total-pressure loss as compared with the solid endwalls, particularly in the vortex core regions, for both cooled-endwall configurations. These losses are somewhat higher for the in-line coolant injection configuration and persist into the vane mean section. This is consistent, as it should be, with the results shown previously for the total-pressure contours of figures 12 and 13. At the higher total-pressure ratios  $p_c/p_0'$  the total-pressure losses decrease, with the 15° to in-line coolant injection configuration being slightly better. The vortex core regions at a total-pressure ratio  $p_c/p_0'$  of 1.8 are significantly modified, particularly in the tip region. The higher momentum of the coolant apparently impedes, to a large extent, the formation of the large passage vortex and the radial migration down the vane trailing-edge region.

### Overall Aerodynamic Performance

**Aftermixed efficiencies.** - The overall aftermixed thermodynamic efficiency,  $\bar{\eta}_{3M,T}$  (eq. (11), appendix) as a function of coolant to primary total-pressure ratio  $p_c/p_0'$  is shown in figure 16 for the two cooled-endwall configurations. The efficiencies are shown as percentages of change (from the solid endwalls) per percentage of coolant. This was done because of the small differences between the two solid-endwall sets (figs. 9 and 10) and the slightly different endwall coolant flow characteristics (fig. 11). Both endwall configurations show similar trends, with the thermodynamic efficiency decreasing with increasing total-pressure ratio  $p_c/p_0'$ . The data for both configurations have been least-squares fit to straight lines in figure 16. Over the range of coolant flow tests, the 15° to in-line coolant injection configuration has a higher efficiency (lower losses) than the in-line configuration. The differences, however, appear to be small even though the two configurations were seen to have larger differences in the endwall regions (figs. 12 to 15). This results from the fact that the overall aftermixed efficiencies represent an "average" for the whole vane and as such tend to mask the differences in the endwall regions. Also, the larger change in efficiency for the in-line coolant injection configuration is offset by larger coolant fractions (fig. 11). At a total-pressure ratio of 1.0, the changes in thermodynamic efficiency per percentage of coolant are -0.760 and -0.737 for the in-line and 15° to in-line coolant injection configurations, respectively.

**Effect of total-temperature ratio.** - As discussed previously, the performance of the cooled endwalls was determined at a primary to coolant total-temperature ratio  $T_0/T_c'$  of 1.0. Although a valid comparison can probably be made at this temperature ratio, it is also of interest to estimate the performance at actual engine conditions. A method for doing this has been described in reference 6. The basic model assumed that the aerodynamic losses (total-pressure losses due to boundary layer growth and mixing) were constant if the coolant to primary momentum ratios (or coolant to primary total-pressure ratios  $p_c/p_0'$  for constant cooling hole areas) were maintained the same for tests at different total-temperature ratios  $T_0/T_c'$ . It was shown (ref. 6) that at a coolant to primary inlet total-pressure ratio  $p_c/p_0'$  of 1, which is representative of actual engine first-stage stator operating conditions, the thermodynamic efficiency is independent of the total-temperature ratio  $T_0/T_c'$ . The coolant fraction  $y_c$  was also shown to vary as the square root of the total-temperature ratio  $T_0/T_c'$  (for constant cooling hole area). Therefore, at the design total-temperature ratio  $T_0/T_c'$  of 2.7 for this stator, the percentages of change in thermodynamic efficiency per percentage of coolant are estimated to be -0.463 (i.e.,  $-0.760/\sqrt{2.7}$ ) and -0.449 for the in-line and the 15° to in-line coolant injection configurations, respectively. These values are somewhat lower than found (ref. 9) for full-film-cooled vanes tested in two-dimensional cascades. If desired, the effect of total-temperature ratio on the performance at other measured total-pressure ratios  $p_c/p_0'$  can also be estimated by the method described in reference 6.

### CONCLUDING REMARKS

At a coolant to primary inlet total-pressure ratio of 1, which is representative of first-stage engine operating conditions, the low-momentum endwall coolants migrated to the passage vortex regions and increased the losses as compared with the solid (un-cooled) endwalls. However, comparing the two cooled-endwall configurations did indicate that the coolant injected at 15° to the inviscid streamline direction was more successful in impeding the secondary flows that can occur in this type of stator. This was seen from the smaller total-pressure losses in the passage vortex regions and by less radial migration of the tip endwall coolant down the trailing-edge region. Further aerodynamic improvements are thought to be possible if the coolant is injected at angles greater than 15° (i.e., 30° or possibly 45°) to the inviscid streamline direction.

More important than aerodynamic gains are the probable implications of the results to the heat transfer characteristics of cooled endwalls in low-aspect-ratio blading. For if the endwall coolant separates and migrates away from the endwalls, the effectiveness of the film cooling will be considerably decreased. Fortunately, recent flow visualization studies (on flat plates) have shown that coolant injected at 45° to the streamwise flow direction tends to prevent the cooling film from separating from the surface even at

ORIGINAL PAGE IS  
OF POOR QUALITY

high blowing rates. In an attempt to use this effect, further aerodynamic tests are currently planned to study the behavior of endwall coolant injected at  $30^\circ$  and  $45^\circ$  to the inviscid streamline direction. Corresponding heat transfer tests are also needed. In addition, it is hoped that the effect of other design parameters (such as hole location, hole size, and blowing rate) on the secondary flows in cooled stators will also be determined. To complement the experimental investigation, theoretical calculation procedures (i.e., endwall boundary layer and three-dimensional viscous computer programs) are currently being developed. These methods should find wide use in the experimental program.

#### SUMMARY OF RESULTS

The performances of two similar endwall cooling configurations were experimentally determined in a cold-air, full-annular cascade, where three-dimensional effects could be obtained. In the first configuration, three rows of cooling holes were oriented so that the endwall coolant was injected in line with the inviscid streamline direction. In the second configuration, the coolant was injected at an angle of  $15^\circ$  to the inviscid streamline direction and oriented toward the vane pressure surface. In both configurations, the coolant was injected at an angle of  $15^\circ$  to the endwall surface. The stator vanes were solid and uncooled so that the effect of endwall cooling could be obtained directly. The investigation was conducted at the vane design, mean-radius, ideal, aftermixed, critical velocity ratio of 0.778. The coolant to primary inlet total-pressure ratios were varied from 1.0 to 2.0, which corresponds to endwall coolant flows from 0.9 to 3.1 percent of primary flow. All tests were conducted at ambient conditions with a primary to coolant inlet total-temperature ratio of 1. Total-pressure contours downstream of the vanes were obtained from survey probe data and were used to determine the effect of endwall cooling on the secondary flows in the stator. The probe data were also used to calculate the overall vane aerodynamic performance. Both cooled-endwall configurations were compared with each other and with the results obtained for the solid (uncooled) endwalls. The results of the investigation were summarized as follows:

1. At a coolant to primary inlet total-pressure ratio of 1, the endwall coolant migrated to the passage vortex regions, increasing the losses as compared with the solid endwalls. The percent changes in the overall thermodynamic efficiency (as compared with the solid endwalls) per percent coolant were -0.760 and -0.737 for the in-line and  $15^\circ$  to in-line coolant injection configurations, respectively.
2. For coolant to primary inlet total-pressure ratios greater than 1, the increased momentum of the endwall coolant improved the secondary flow characteristics (decreased total-pressure losses and underturning in the passage vortex regions) of the whole vane.
3. The  $15^\circ$  to in-line coolant injection configuration was more successful in impeding the vane secondary flows and, therefore, had somewhat better aerodynamic performance than did the in-line coolant injection configuration over the range of coolant flows investigated.

ORIGINAL PAGE IS  
OF POOR QUALITY

APPENDIX - CALCULATION OF AFTERMIXED CONDITIONS AND VANE EFFICIENCY  
FROM SURVEY MEASUREMENTS

The aftermixed conditions (station 3M) are obtained from the survey measurements by applying the conservation equations to an annular-sector control volume of infinitesimal radial thickness as shown in figure 17. The stream surfaces downstream of the vanes are assumed to be cylindrical because of the axial character of the annular cascade. In application of the conservation equations, it is also assumed that the viscous terms are negligible and that the pressure terms on the side faces of the control volume cancel due to symmetry.

The conservation of mass requires that

$$\int_0^\theta \rho_3(r, \theta) V_{3,z}(r, \theta) d\theta = \rho_{3M}(r) V_{3M,z}(r) \theta \equiv \bar{m}(r) \quad (1)$$

The conservation of momentum gives

$$\int_0^\theta [\rho_3(r, \theta) V_{3,z}^2(r, \theta) + g p_3(r)] d\theta = [\rho_{3M}(r) V_{3M,z}^2(r) + g p_{3M}(r)] \theta \equiv J_z(r) \bar{m}(r) \quad (2)$$

$$\int_0^\theta [\rho_3(r, \theta) V_{3,z}(r, \theta) V_{3,\theta}(r, \theta)] d\theta = [\rho_{3M}(r) V_{3M,z}(r) V_{3M,\theta}(r)] \theta \equiv J_\theta(r) \bar{m}(r) \quad (3)$$

The energy equation for the special case of equal coolant and primary total temperatures is

$$C_p T_3(r, \theta) + \frac{V_3^2(r, \theta)}{2gJ} = C_p T_{3M}(r) + \frac{V_{3M}^2(r)}{2gJ} = C_p T'_{3M} = C_p T'_0 \equiv E = \text{Constant} \quad (4)$$

The perfect-gas relation completes the system of equations

$$\rho_{3M}(r) = \frac{p_{3M}(r)}{RT_{3M}(r)} \quad (5)$$

Solving for the axial velocity  $V_{3M,z}(r)$  gives (ref. 8)

$$V_{3M,z}(r) = \frac{\gamma}{\gamma + 1} J_z(r) - \sqrt{\left[ \frac{\gamma}{\gamma + 1} J_z(r) \right]^2 - \frac{\gamma - 1}{\gamma + 1} [2gJE - J_\theta^2(r)]} \quad (6)$$

The tangential velocity  $V_{3M,\theta}(r)$  is obtained from equation (3)

$$V_{3M,\theta}(r) = J_\theta(r) \quad (7)$$

and the velocity  $V_{3M}(r)$  from

$$V_{3M}(r) = \sqrt{V_{3M,z}^2(r) + V_{3M,\theta}^2(r)} \quad (8)$$

The aftermixed conditions of density  $\rho_{3M}(r)$ , static temperature  $T_{3M}(r)$ , and static pressure  $p_{3M}(r)$  are found from equations (1), (4), and (5), respectively. The aftermixed total pressure  $p_{3M}^*$  is then obtained from

$$\frac{p_{3M}^*}{p_{3M}(r)} = \left[ 1 + \frac{\gamma - 1}{2} M_{3M}^2(r) \right]^{\gamma/(\gamma-1)} \quad (9)$$

where

$$M_{3M}(r) = \frac{V_{3M}(r)}{\sqrt{\gamma g R T_{3M}(r)}} \quad (10)$$

The aftermixed conditions have been determined in terms of the parameters  $\bar{m}(r)$ ,  $J_z(r)$ ,  $J_\theta(r)$ , and  $E$ , which are calculated from the survey measurements.

The aftermixed thermodynamic efficiency is defined as the ratio of the actual aftermixed kinetic energy to the sum of the ideal aftermixed kinetic energies of both the primary and coolant flows. The thermodynamic efficiency for the total vane passage

is

$$\bar{n}_{3M,T} = \frac{\int_{r_i}^{r_o} [\rho_{3M}(r) v_{3M,z}(r) v_{3M}^2(r)] r dr}{\int_{r_i}^{r_o} \rho_{3M}(r) v_{3M,z}(r) \left\{ y_p(r) [v_{3M,id}^2(r)]_p + y_{c,h}(r) [v_{3M,id}^2(r)]_{c,h} + y_{c,t}(r) [v_{3M,id}^2(r)]_{c,t} \right\} r dr} \quad (11)$$

where the ideal velocities are given by

$$[v_{3M,id}(r)]_p = \sqrt{\left(\frac{2\gamma}{\gamma-1}\right) gRT'_0 \left\{ 1 - \left[\frac{P_{3M}(r)}{P_0}\right]^{(\gamma-1)/\gamma} \right\}} \quad (12)$$

$$[v_{3M,id}(r)]_{c,h} = \sqrt{\left(\frac{2\gamma}{\gamma-1}\right) gRT'_{c,h} \left\{ 1 - \left[\frac{P_{3M}(r)}{P_{c,h}}\right]^{(\gamma-1)/\gamma} \right\}} \quad (13)$$

$$[v_{3M,id}(r)]_{c,t} = \sqrt{\left(\frac{2\gamma}{\gamma-1}\right) gRT'_{c,t} \left\{ 1 - \left[\frac{P_{3M}(r)}{P_{c,t}}\right]^{(\gamma-1)/\gamma} \right\}} \quad (14)$$

The total pressure at the bellmouth inlet  $p'_0$  was used (instead of  $p_j$ ) to calculate the ideal velocity of the primary flow (eq. (12)). This was done because the vane inlet total pressure  $p_j(r)$  was measured only for the solid endwall tests of the in-line coolant injection vane rings and because of its negligible effect on the results. The fraction of coolant flow to total flow was assumed to be independent of radius and equal to

$$y_{c,h}(r) = \frac{\bar{m}_{c,h}}{\bar{m}} = \text{Constant} \quad (15)$$

$$y_{c,t}(r) = \frac{\bar{m}_{c,t}}{\bar{m}} = \text{Constant} \quad (16)$$

$$y_p(r) = 1 - [y_{c,h}(r) + y_{c,t}(r)] = \text{Constant} \quad (17)$$

where  $\bar{m}_{c,h}$  and  $\bar{m}_{c,t}$  are the measured total coolant flow rates per passage for the hub and tip endwall coolants, respectively. And  $\bar{m}$  is the total flow rate per passage and is given by

$$\bar{m} = \int_{r_h}^{r_t} \int_0^\theta \rho_3(r,\theta) v_{3,z}(r,\theta) r d\theta dr = \int_{r_h}^{r_t} \bar{m}(r) r dr \quad (18)$$

#### REFERENCES

1. Szanca, Edward M., Schum, Harold J., and Hotz, Glen M., "Research Turbine for High-Temperature Core Engine Application. I - Cold-Air Overall Performance of Solid Scaled Turbine," NASA TN D-7557, February 1974.
2. Stabe, Roy G., and Kline, John F., "Aerodynamic Performance of a Core-Engine Turbine Stator Vane Tested in a Two-Dimensional Cascade of 10 Vanes and in a Single-Vane Tunnel," NASA TM X-2766, March 1973.
3. Goldman, Louis J., and McLallin, Kerry L., "Cold-Air Annular-Cascade Investigation of Aerodynamic Performance of Core-Engine-Cooled Turbine Vanes. I - Solid-Vane Performance and Facility Description," NASA TM X-3224, April 1975.
4. McDonel, J. D., et al., "Core Turbine Aerodynamic Evaluation - Test Data From Initial Turbine," NASA CR-2596, February 1976.
5. Colladay, Raymond S., and Russell, Louis M., "Streakline Flow Visualization of Discrete Hole Film Cooling for Gas Turbine Applications," Journal of Heat Transfer, Vol. 98, No. 2, May 1976, pp. 245-250.
6. Goldman, Louis J., "Cooled-Turbine Aerodynamic Performance Prediction from Reduced Primary to Coolant Total-Temperature-Ratio Results," NASA TN D-8312, October 1976.
7. Krause, Lloyd N., and Gettelman, Clarence C., "Considerations Entering into the Selection of Probes for Pressure Measurements in Jet Engines," Instrument Society of America Proceedings. Vol. 7, 1952, pp. 134-137.
8. Goldman, Louis J., and McLallin, Kerry L., "Cold-Air Annular-Cascade Investigation of Aerodynamic Performance of Cooled Turbine Vanes. I - Facility Description and Base (Solid) Vane Performance," NASA TM X-3006, March 1974.
9. Moffitt, Thomas P., Stepka, Francis S., and Rohlik, Harold E., "Summary of NASA Aerodynamic and Heat Transfer Studies in Turbine Vanes and Blades," SAE Paper 760917, 1976.

TABLE I. - ENDWALL COOLING HOLE COORDINATES

Cooling hole	(a) Hub wall				(b) Tip wall													
	X (fig. 5)		Y (fig. 5)		X (fig. 5)		Y (fig. 5)		A (fig. 5), deg									
	cm	in.	cm	in.	cm	in.	cm	in.	Con-figuration 1a	Con-figuration 2b								
1	2.433	0.958	2.350	0.925	56.67	71.67	2.840	1.118	-0.193	-0.076	75.00	90.00	45	-0.419	4.293	1.690	-34.00	-34.00
2	2.586	1.018	2.088	.822	58.42	73.42	2.764	1.088	-.320	-.126	-70.58	-85.58	46	-.419	4.031	1.587	-34.00	-34.00
c3	2.738	1.078	1.829	.720	59.08	74.08	2.680	1.055	-.457	-.180	-70.58	-85.58	47	-.419	3.769	1.484	-34.00	-34.00
c4	2.891	1.138	1.560	.614	60.75	75.75	2.601	1.024	-.584	-.230	-65.42	-80.42	48	-.419	3.510	1.382	-34.00	-34.00
c5	3.043	1.198	1.300	.512	66.25	81.25	2.520	.992	-.721	-.284	-63.25	-78.25	49	-.419	3.249	1.279	-34.00	-34.00
c6	3.195	1.258	1.036	.408	72.67	87.67	2.438	.960	-.848	-.334	-59.83	-74.83	50	-.419	2.987	1.176	-34.00	-34.00
c7	3.348	1.318	.777	.306	90.00	---	2.357	.928	-.980	-.386	-58.17	-73.17	51	-.419	2.728	1.074	-34.00	-34.00
8	1.331	.524	1.179	.464	39.42	54.42	2.276	.896	-1.113	-.438	-56.25	-71.25	52	-.419	2.466	.971	-34.00	-34.00
9	1.519	.598	1.031	.406	39.42	54.42	2.200	.866	-1.234	-.486	-52.92	-67.92	53	-.419	2.205	.868	-34.00	-34.00
10	1.717	.676	.869	.342	41.08	56.08	2.118	.834	-1.367	-.538	-48.50	-63.50	54	-.419	1.946	.766	-34.00	-34.00
11	1.915	.754	.711	.280	45.92	60.92	2.037	.802	-1.494	-.588	-48.50	-63.50	55	-.419	1.684	.663	-34.00	-34.00
12	2.113	.832	.554	.218	52.58	67.58	1.966	.774	-1.621	-.638	-48.50	-63.50	56	-.419	1.422	.560	-34.00	-34.00
13	3.345	1.336	-.041	-.058	33.17	48.17	1.875	.738	-1.765	-.695	-46.92	-61.92	57	-.419	1.163	.458	-34.00	-34.00
14	.523	.206	-.147	-.100	33.17	48.17	1.463	.576	.671	-.264	-36.00	-51.00	58	-.419	.902	.355	-34.00	-34.00
15	.701	.276	-.254	-.100	33.17	48.17	1.341	.528	.579	.228	-36.00	-51.00						
16	.879	.346	-.361	-.142	33.17	48.17	1.219	.480	.483	.190	-36.00	-51.00						
17	1.057	.416	-.467	-.184	33.17	48.17	1.097	.432	.396	.156	-36.00	-51.00						
18	.325	.128	-.269	-.106	33.17	48.17	.975	.384	.300	.118	-36.00	-51.00						
19	.503	.198	-.376	-.148	33.17	48.17	.853	.336	.213	.084	-36.00	-51.00						
20	.681	.268	-.483	-.190	33.17	48.17	.737	.290	.122	.048	-36.00	-51.00						
21	.859	.338	-.589	-.232	33.17	48.17	.610	.240	.030	.012	-36.00	-51.00						
c22	1.036	.408	-.696	-.274	33.17	48.17	.493	.194	-.066	-.026	-36.00	-51.00						

<sup>a</sup>Cooling holes in line with inviscid streamlines.

<sup>b</sup>Cooling holes at 15° to inviscid streamlines and directed toward vane pressure surface.

<sup>c</sup>Cooling holes could not be machined in configuration 2. Holes filled with epoxy in configuration 1.

<sup>d</sup>Cooling holes could not be machined in configurations 1 and 2.

PREVIOUS PAGE IS  
FINE QUALITY

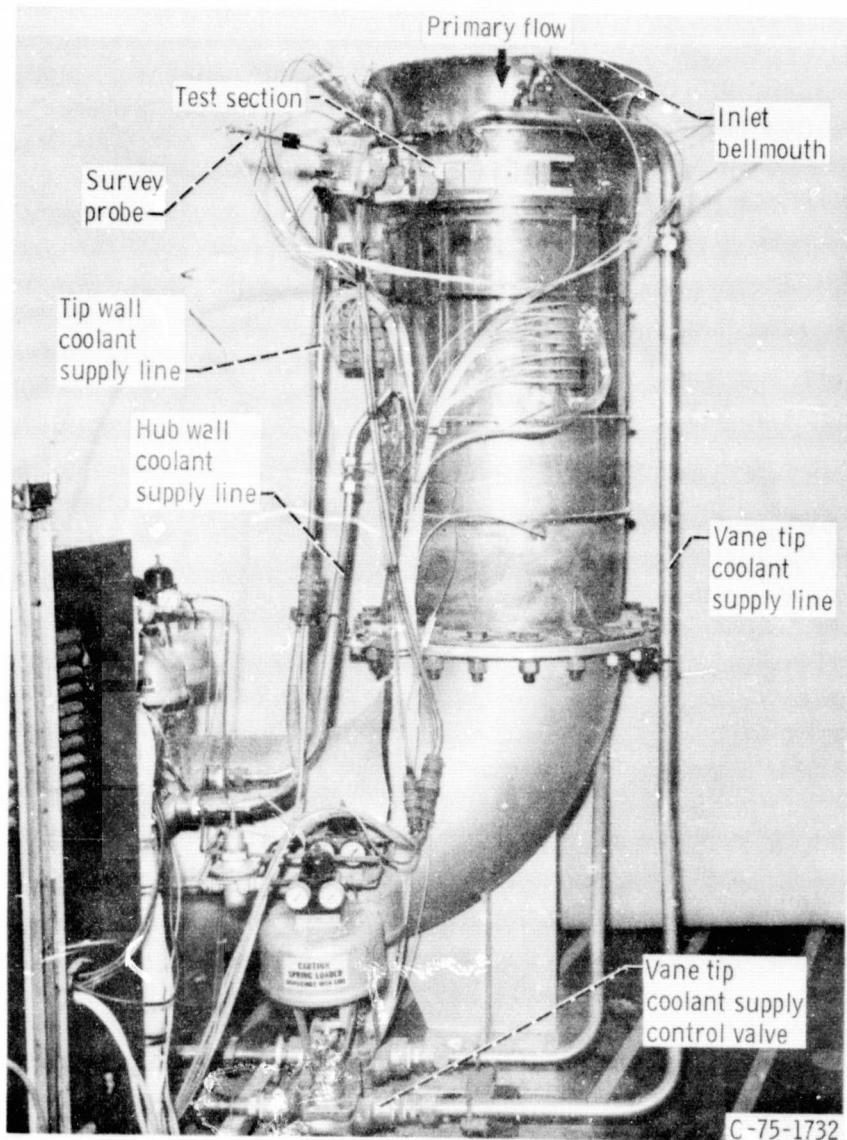


Figure 1. - Core-turbine stator annular cascade.

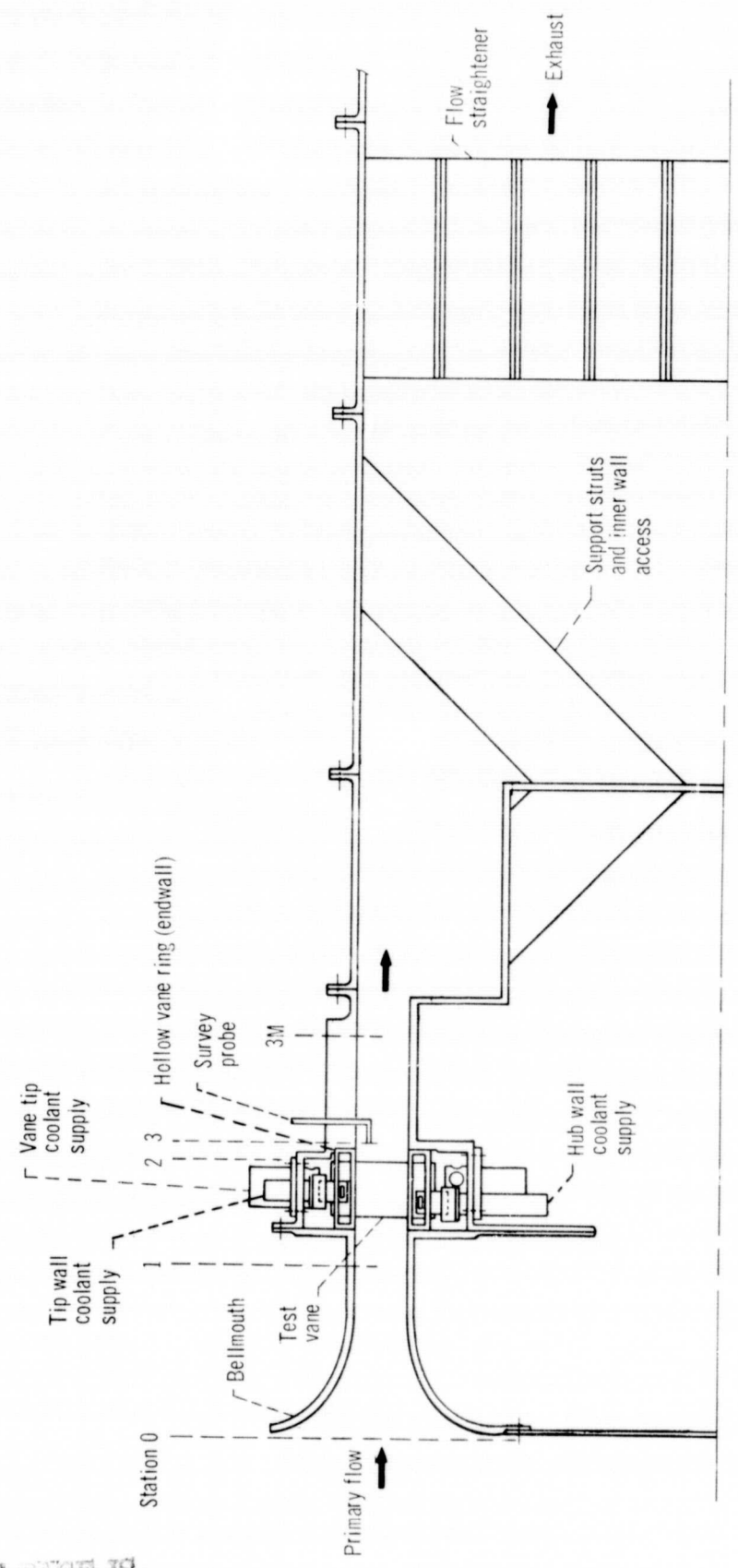


Figure 2. - Schematic cross-sectional view of core-turbine stator cascade.



X		Y <sub>L</sub>		Y <sub>U</sub>	
cm	in.	cm	in.	cm	in.
0	0	0.508	0.200	0.508	0.200
0.127	0.050	---	---	.851	.335
.254	.100	---	---	1.003	.395
.381	.150	---	---	1.120	.441
.508	.200	---	---	1.212	.477
.635	.250	---	---	1.285	.506
.762	.300	.061	.024	1.341	.528
.889	.350	.117	.046	1.389	.547
1.016	.400	.163	.064	1.425	.561
1.143	.450	.201	.079	1.448	.570
1.270	.500	.236	.093	1.463	.576
1.397	.550	.267	.105	1.471	.579
1.524	.600	.292	.115	1.476	.581
1.778	.700	.328	.129	1.461	.575
2.032	.800	.358	.141	1.427	.562
2.286	.900	.376	.148	1.377	.542
2.540	1.000	.384	.151	1.321	.520
2.794	1.100	.381	.150	1.255	.494
3.048	1.200	.368	.145	1.191	.469
3.302	1.300	.353	.139	1.110	.437
3.556	1.400	.328	.129	1.026	.404
3.810	1.500	.297	.117	.942	.371
4.064	1.600	.262	.103	.848	.334
4.318	1.700	.221	.087	.747	.294
4.572	1.800	.178	.070	.635	.250
4.826	1.900	.130	.051	.521	.205
5.080	2.000	.084	.033	.399	.157
5.334	2.100	.025	.010	.267	.105
5.552	2.186	.089	.035	.089	.035

$$(V/V_{cr})_{id,1} = 0.231$$

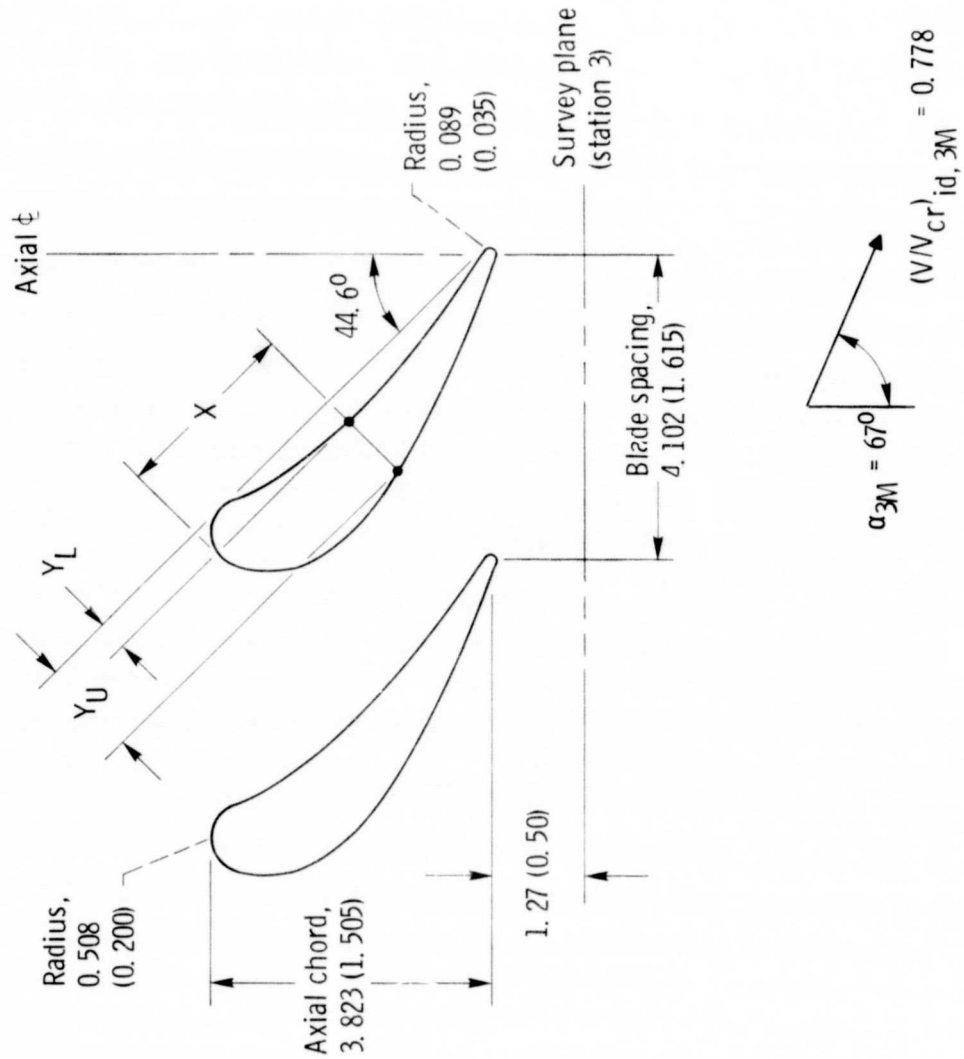
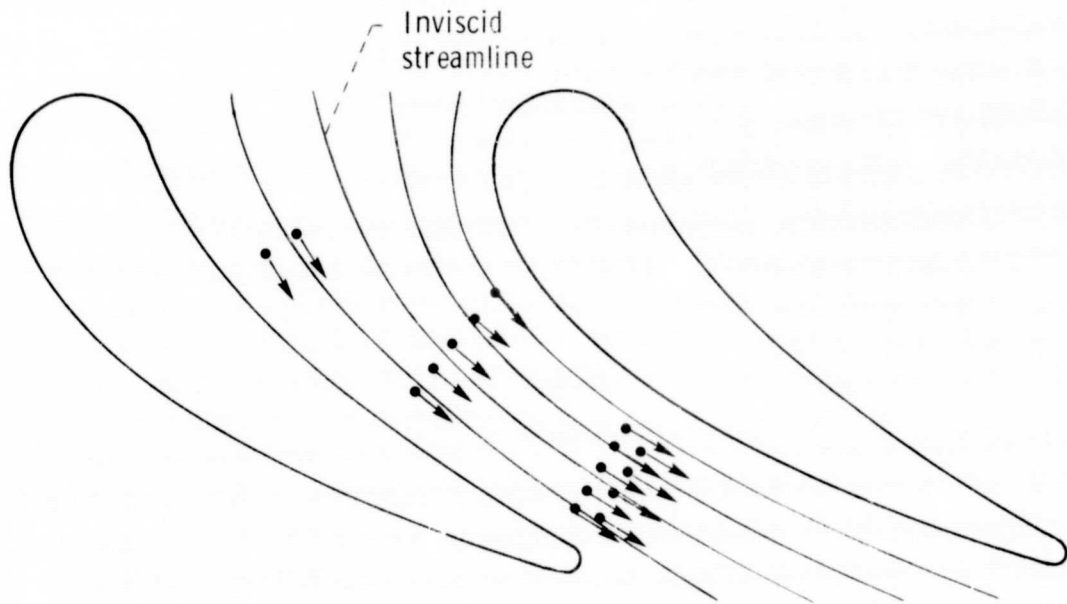
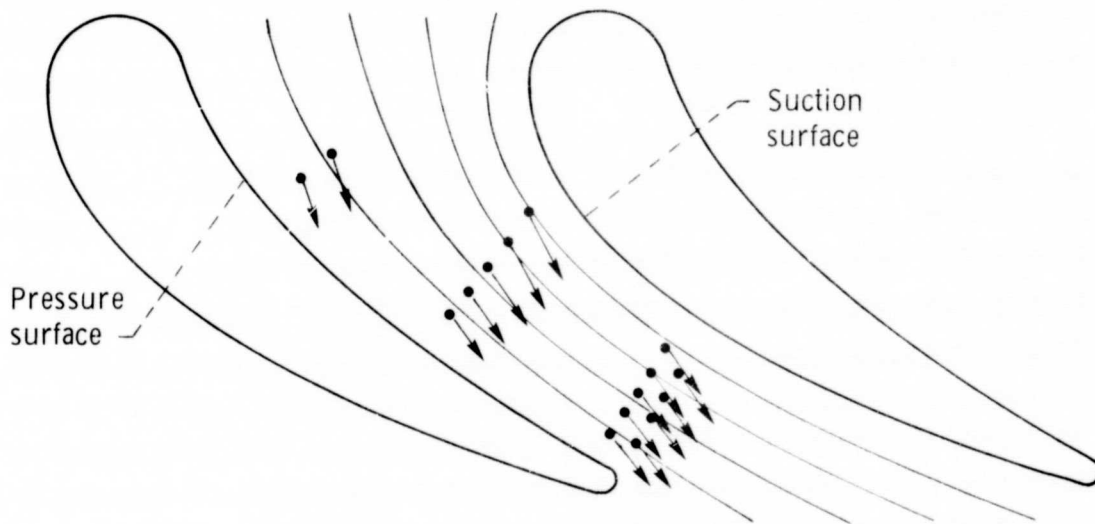


Figure 3. - Core-turbine stator vane geometry at mean section. (All dimensions in cm (in.) except as noted.)



(a) Coolant injected in line with inviscid streamlines.



(b) Coolant injected at  $15^\circ$  to inviscid streamlines and directed toward pressure surface.

Figure 4. - Schematic of two cooled-endwall configurations (showing hub wall only).

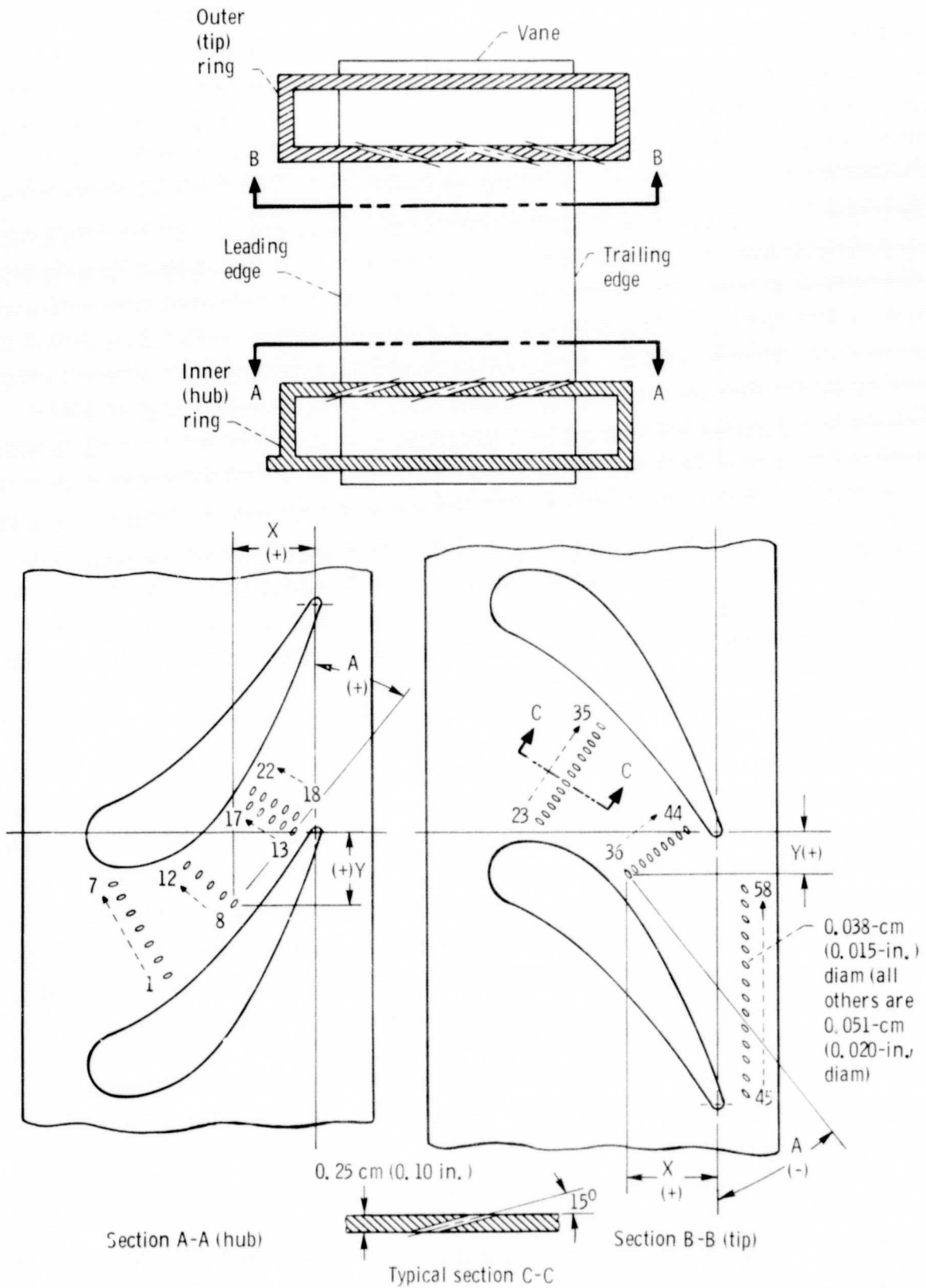
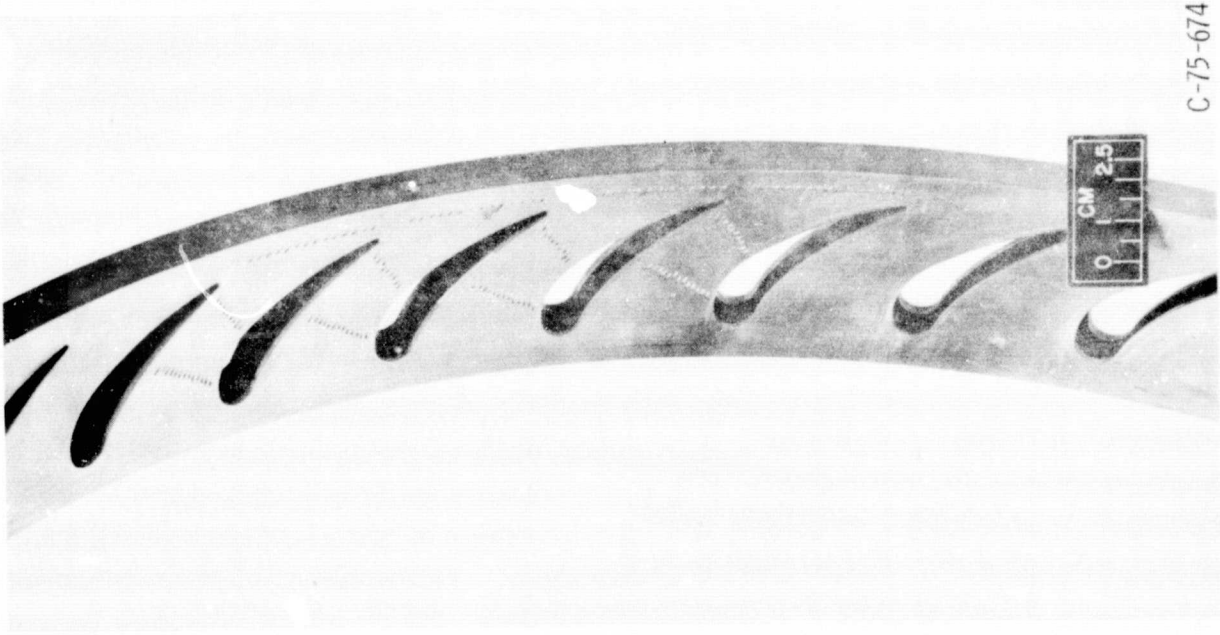


Figure 5. - Schematic of endwall cooling geometry.



(a) Hub.



(b) Tip.

Figure 6. - Hollow vane rings showing endwall cooling pattern.

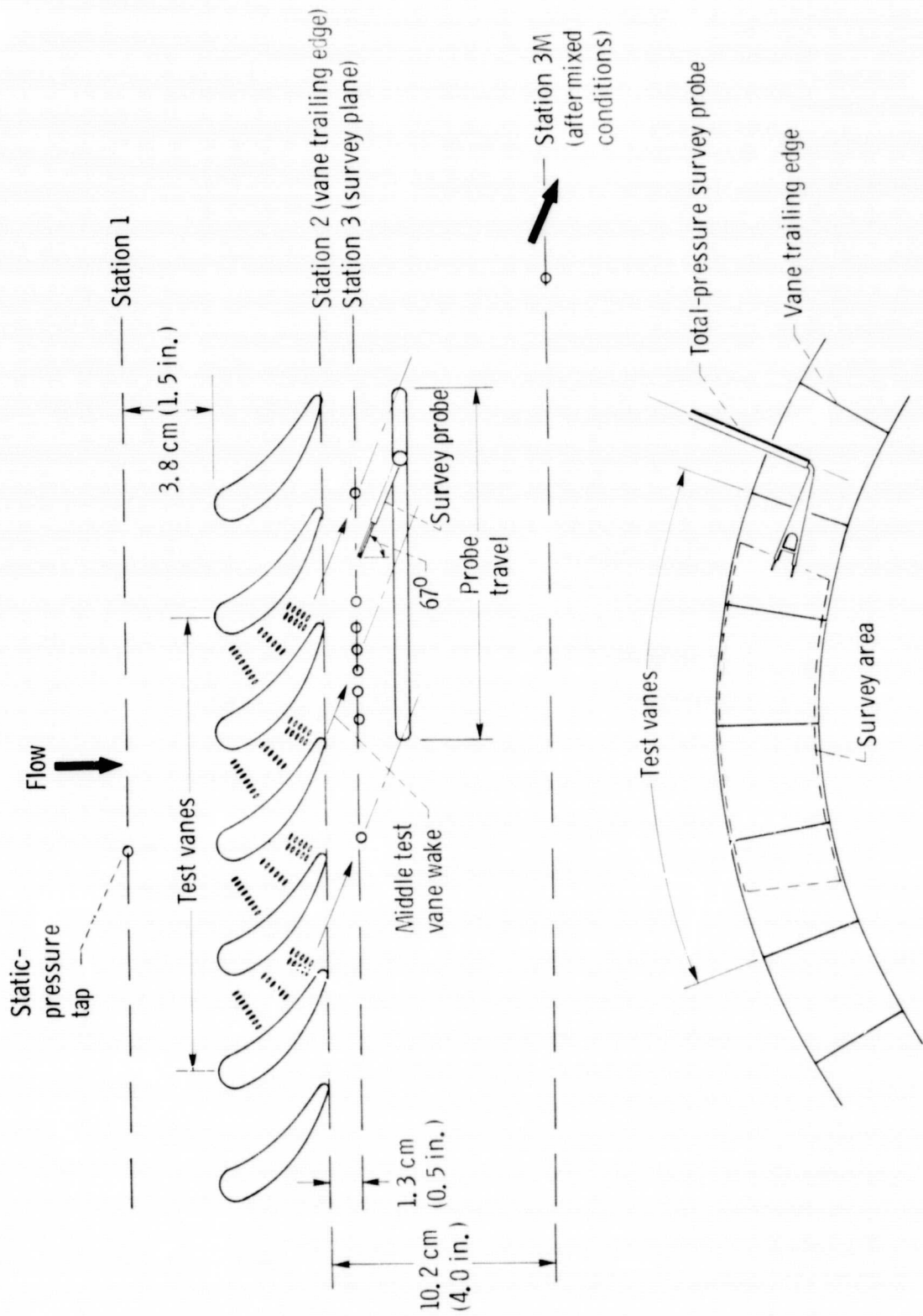


Figure 7. - Schematic of instrumentation for survey data.

E-8988

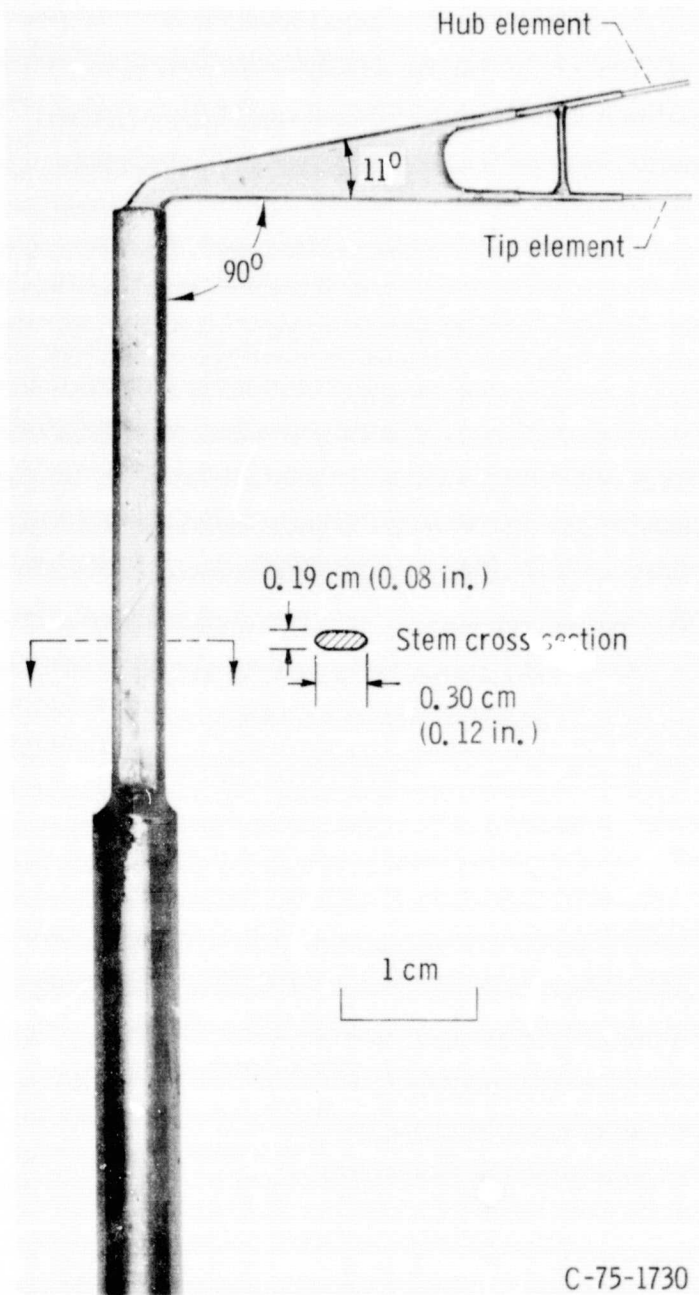
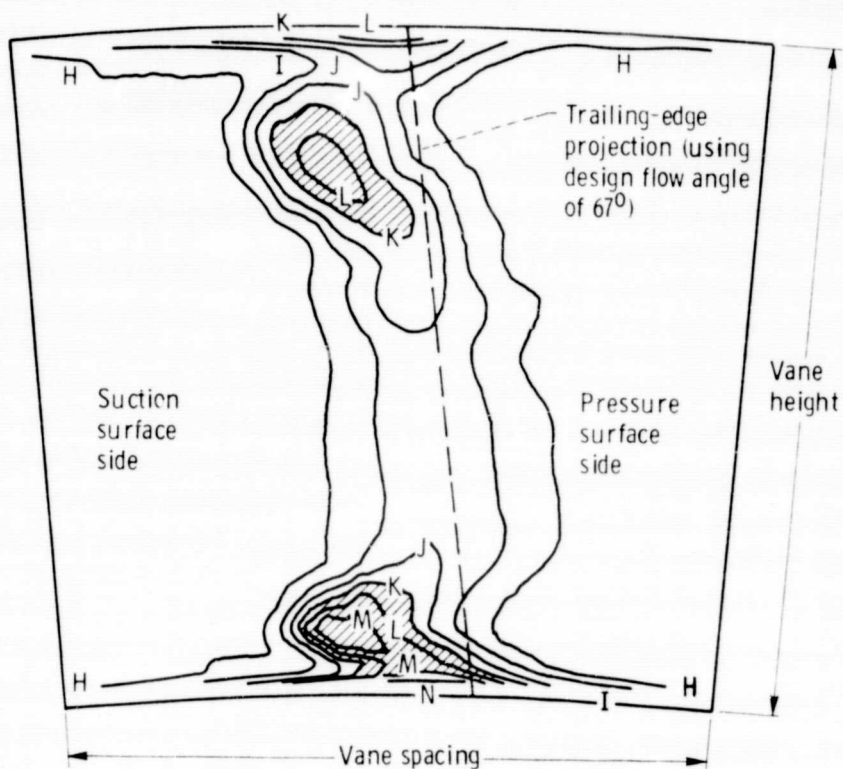
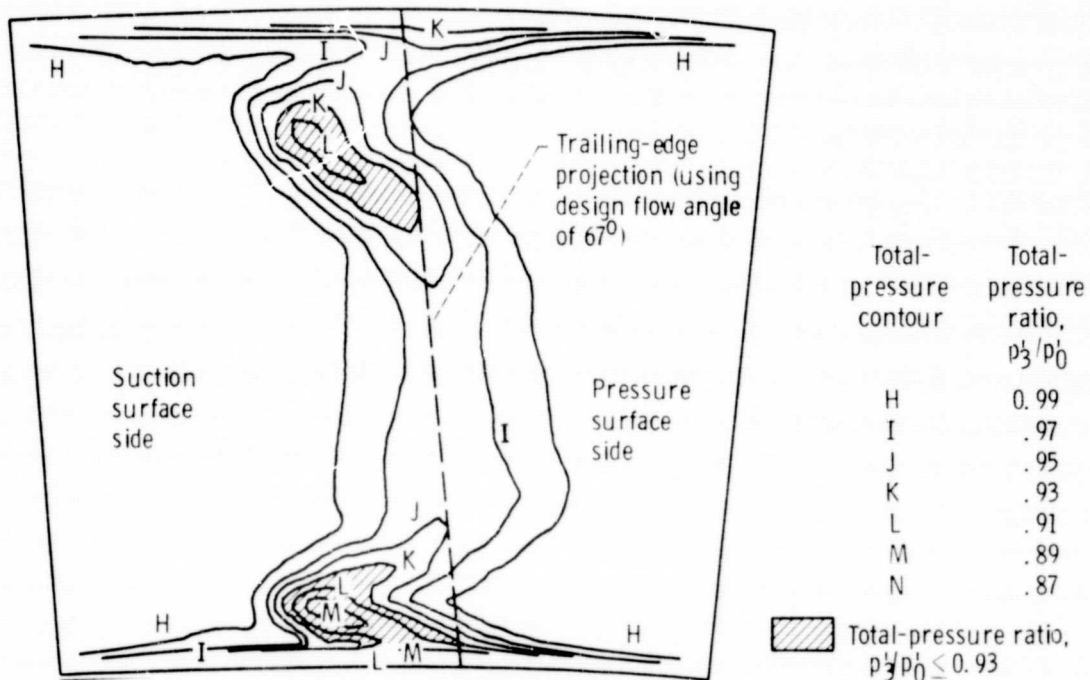


Figure 8. - Total-pressure survey probe.



(a) Solid vanes and endwalls used for subsequent tests of endwall coolant injected in line with inviscid streamlines.



(b) Solid vanes and endwalls used for subsequent tests of endwall coolant injected at  $15^\circ$  to inviscid streamlines.

Figure 9. - Comparison of survey plane total-pressure contour plots of two sets of solid (uncooled) vanes and endwalls used for subsequent cooled-endwall tests.



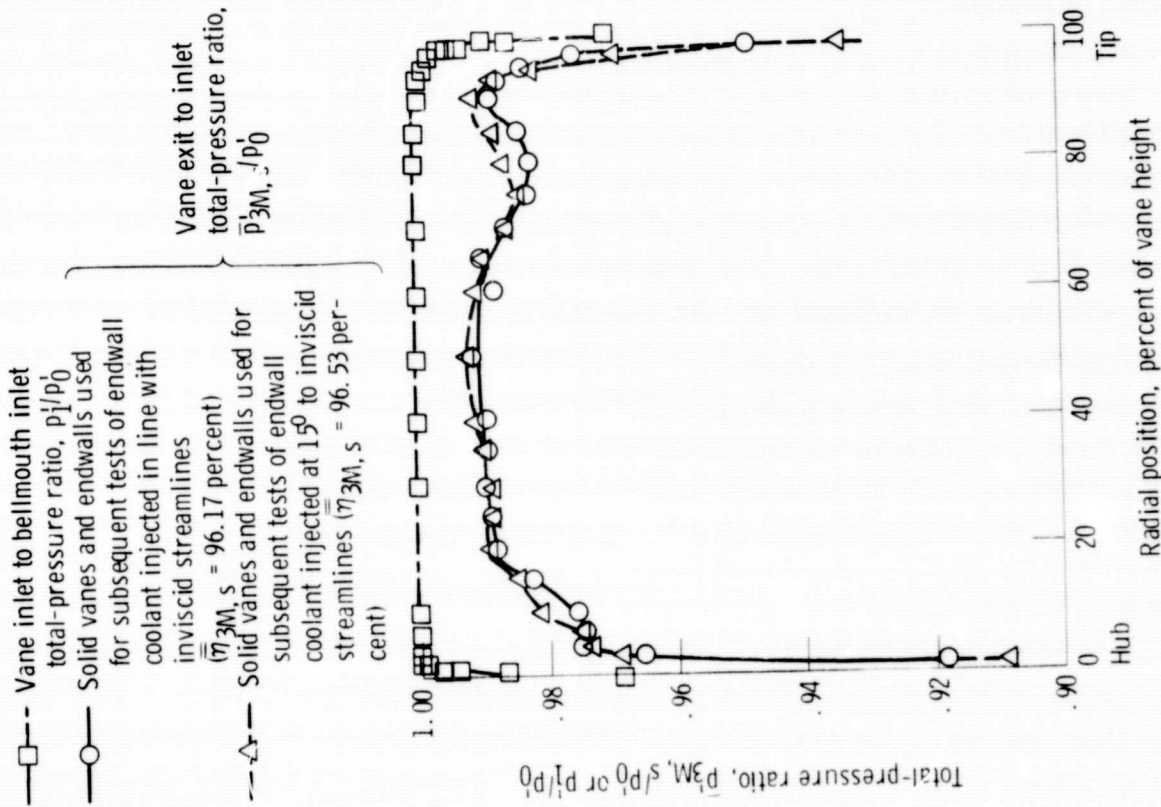


Figure 10. - Comparison of vane exit characteristics for two sets of solid (uncooled) vanes and endwalls used for subsequent cooled-endwall tests.

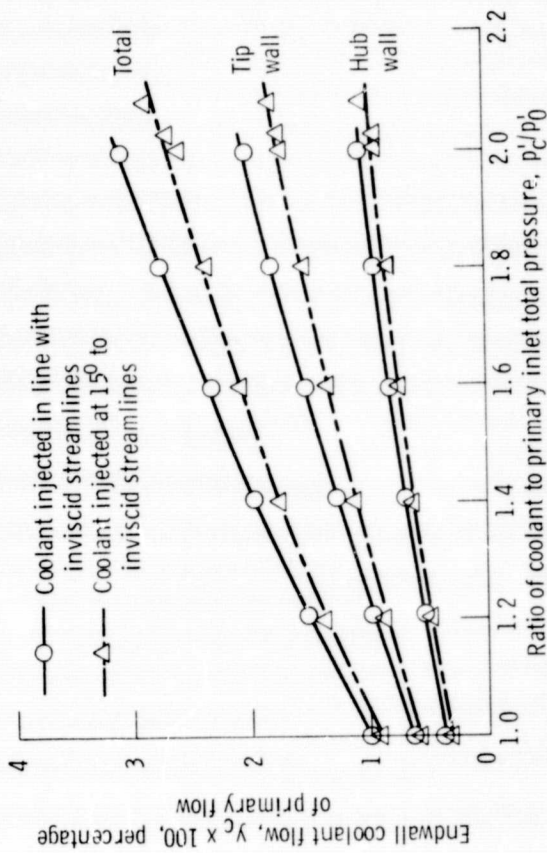
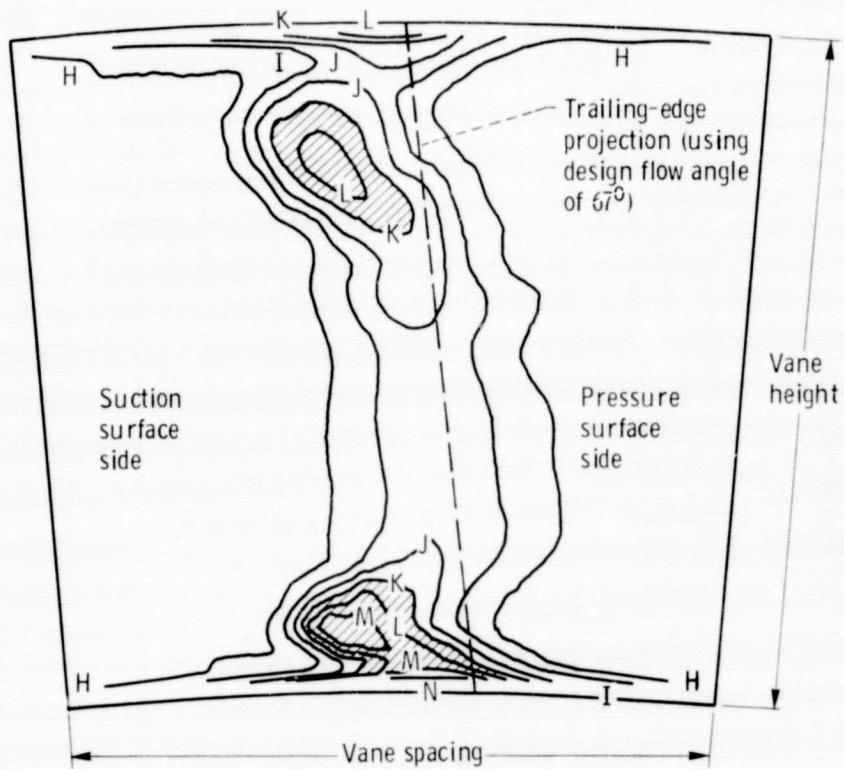
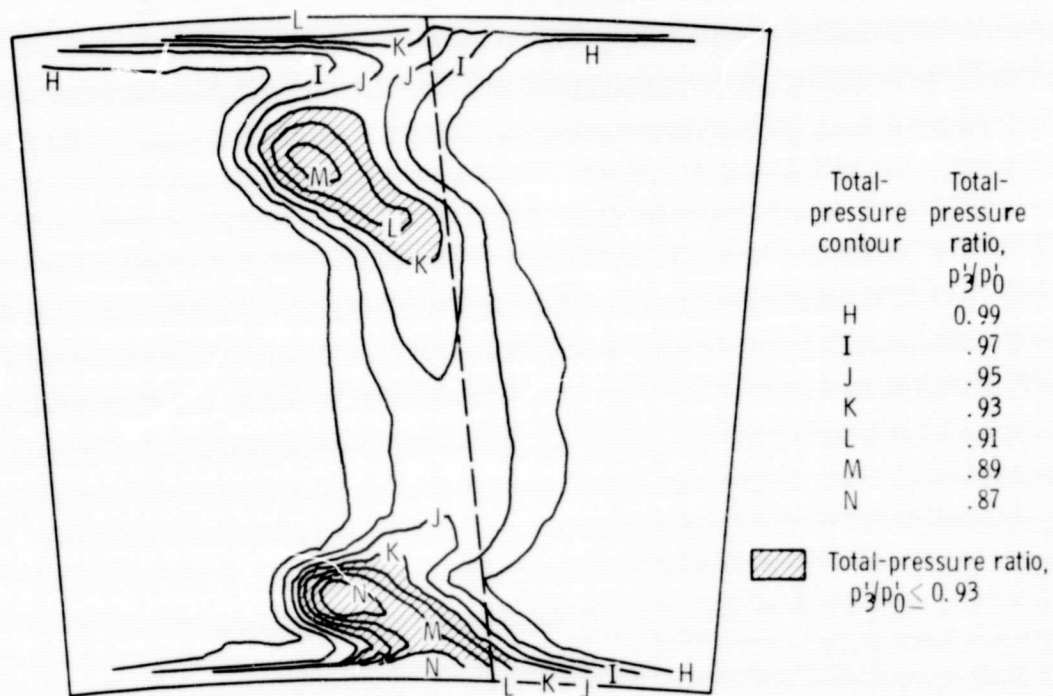


Figure 11. - Coolant flow as function of coolant to primary inlet total-pressure ratio for two cooled-endwall configurations.



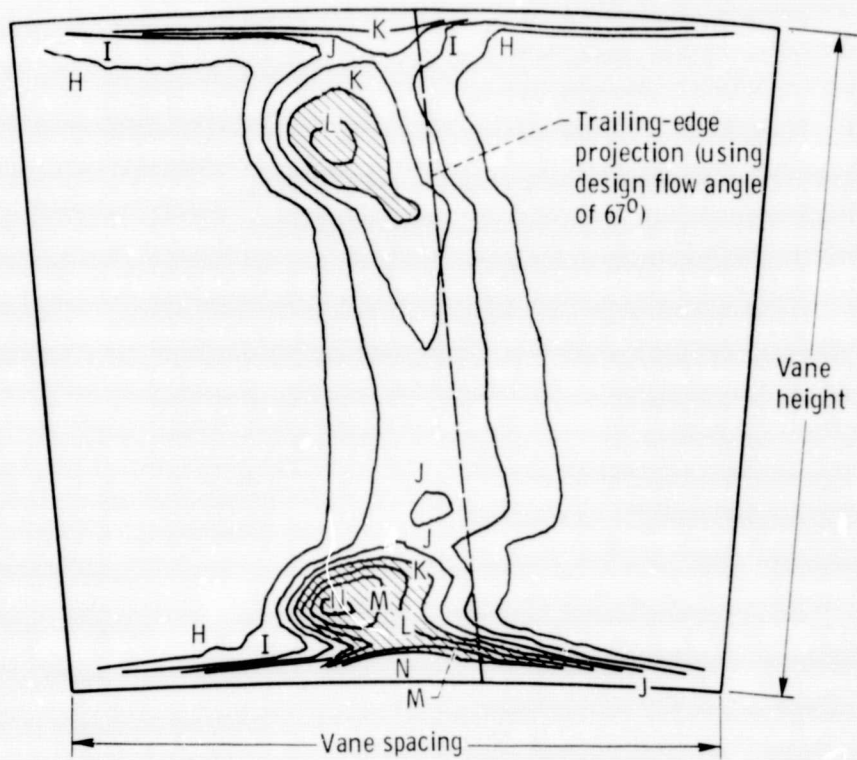


(a) Solid (uncooled) vanes and endwalls.

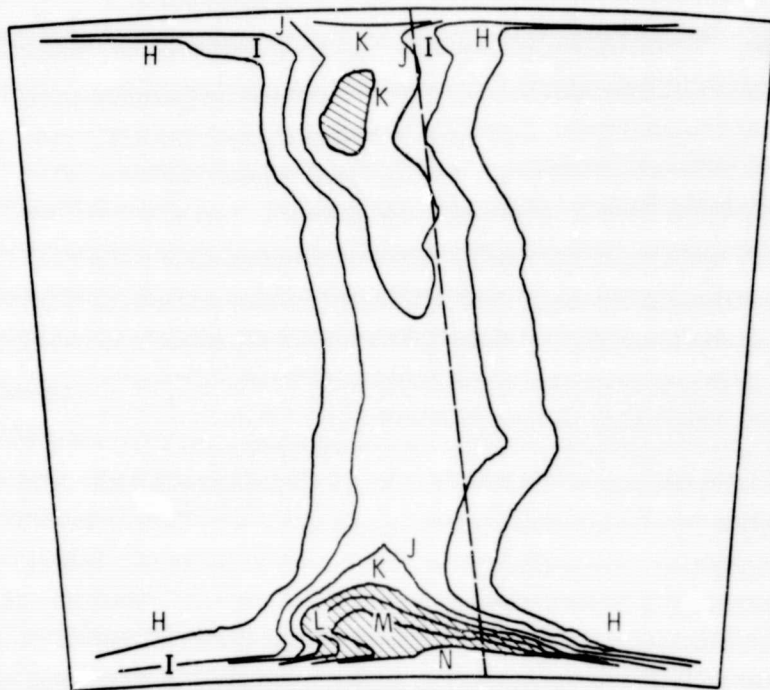


(b) Coolant to inlet total-pressure ratio,  $p_c^*/p_0^*$ , 1.0.


Figure 12. - Survey plane total-pressure ratio contour plots for endwall coolant injected in line with inviscid streamline direction.



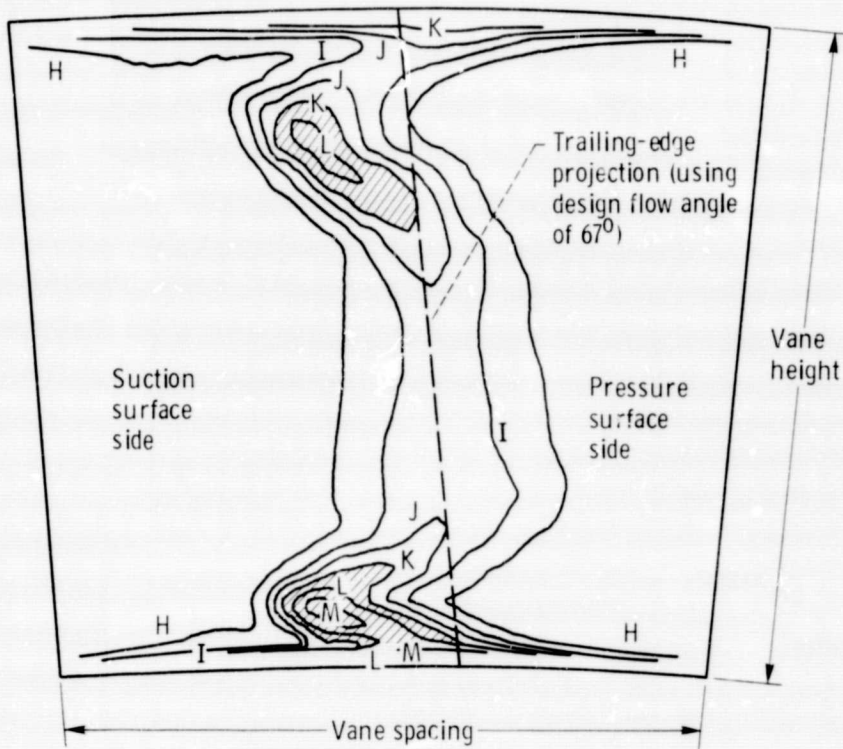
(c) Coolant to inlet total-pressure ratio,  $p_c'/p_0'$ , 1.4.



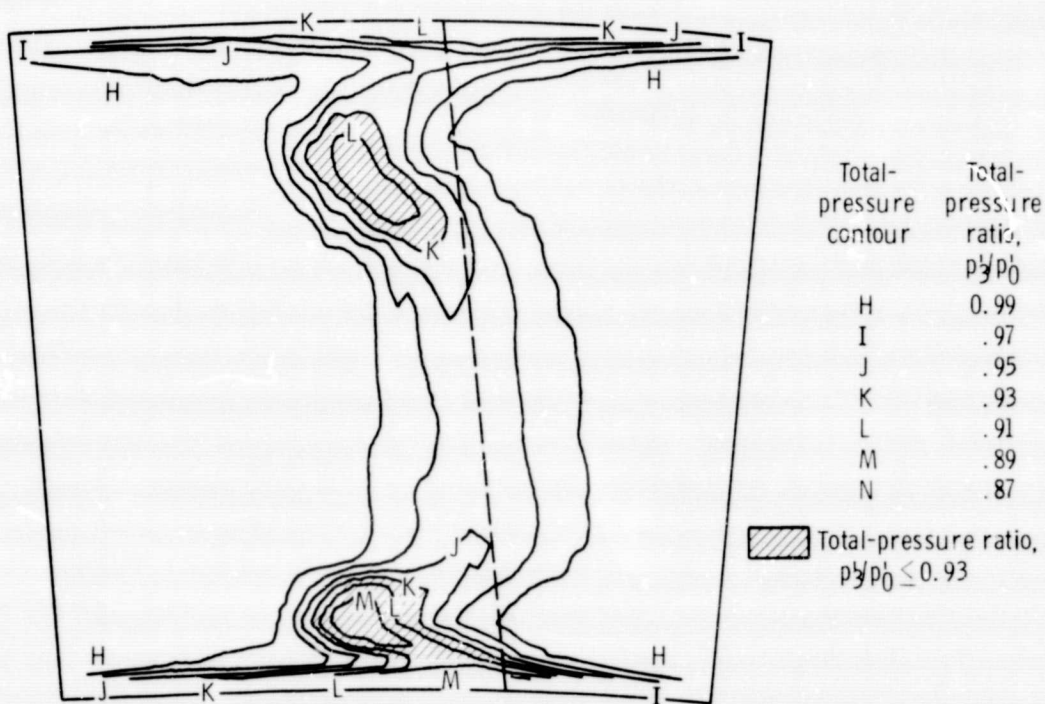
Total-pressure contour	Total-pressure ratio, $p_c'/p_0'$
H	0.99
I	.97
J	.95
K	.93
L	.91
M	.89
N	.87

 Total-pressure ratio,  $p_c'/p_0' \leq 0.93$

(d) Coolant to inlet total-pressure ratio,  $p_c'/p_0'$ , 1.8.

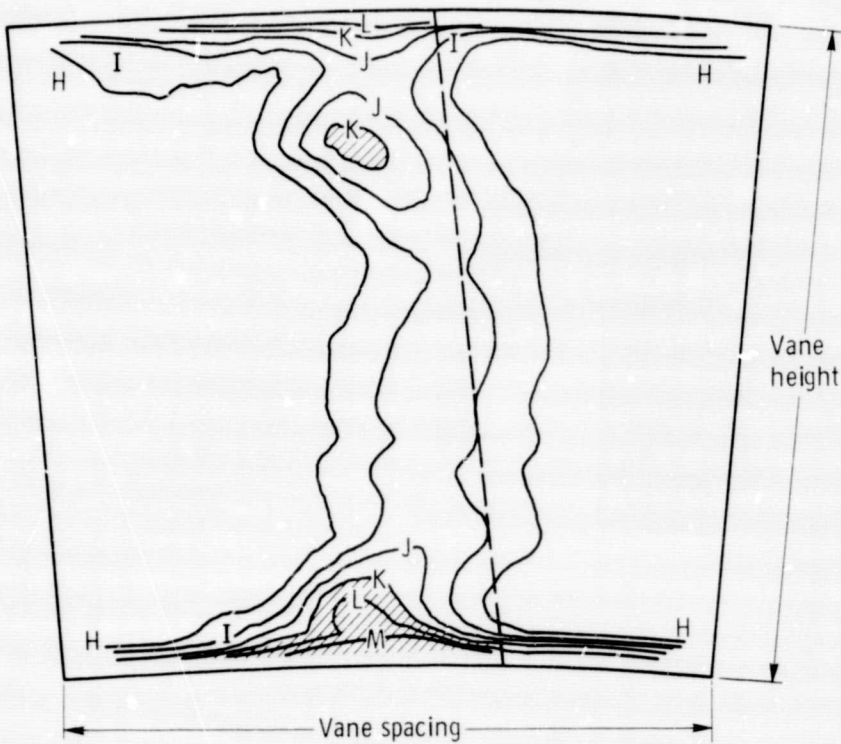


(a) Solid (uncooled) vanes and endwalls.

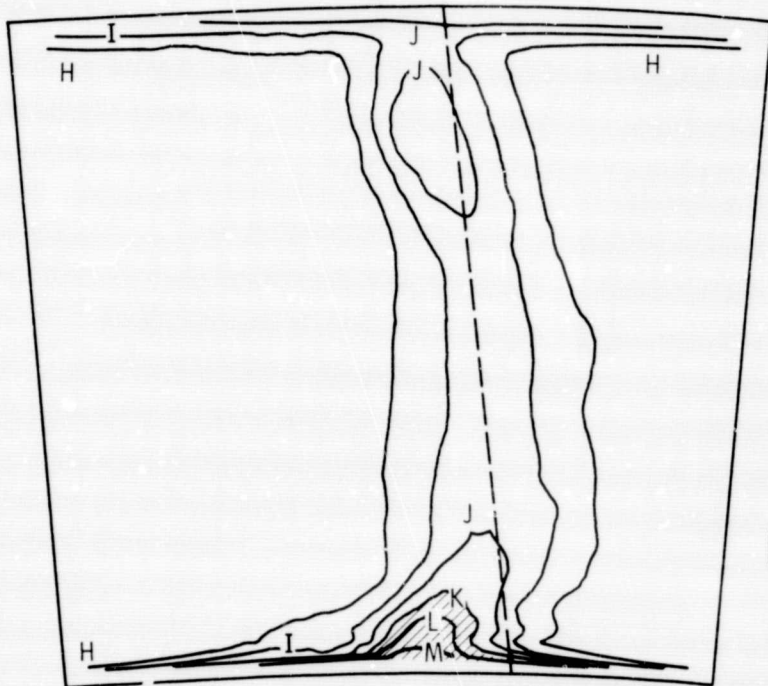


(b) Coolant to inlet total-pressure ratio,  $p_c^*/p_0^*$ , 1.0.

Figure 13. - Survey plane total-pressure ratio contour plots for endwall coolant injected at  $15^\circ$  to inviscid streamline direction and oriented toward pressure surface.



(c) Coolant to inlet total-pressure ratio,  $p_c^i/p_0^i$ , 1.4.



Total-pressure contour	Total-pressure ratio, $p^i/p_0^i$
H	0.99
I	.97
J	.95
K	.93
L	.91
M	.89
N	.87

Total-pressure ratio,  $p^i/p_0^i \leq 0.93$

(d) Coolant to inlet total-pressure ratio,  $p_c^i/p_0^i$ , 1.8.

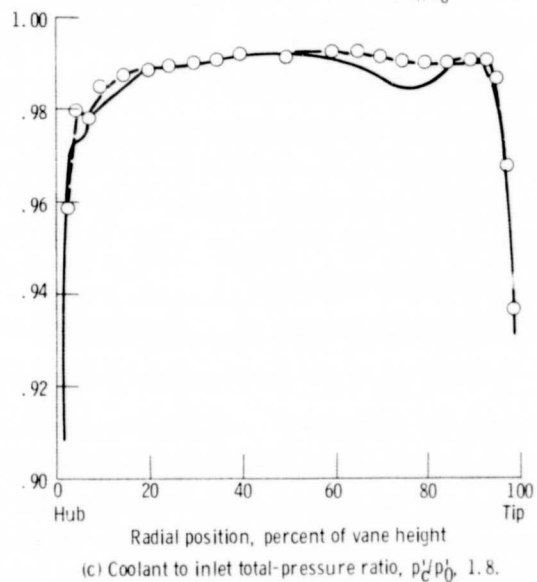
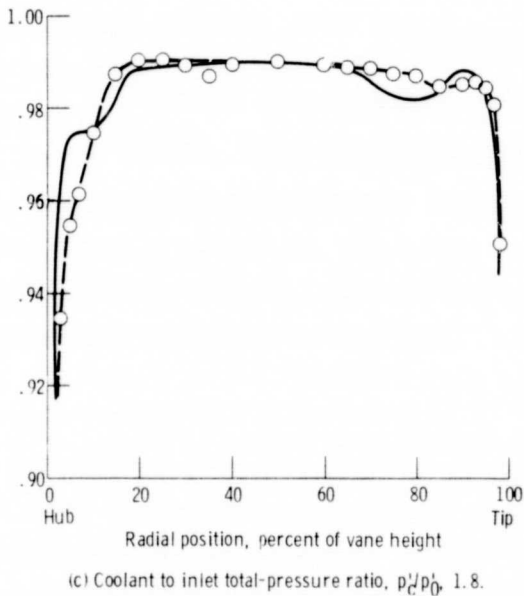
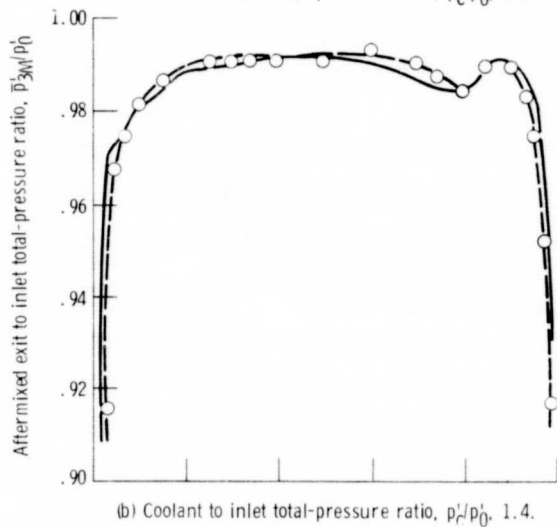
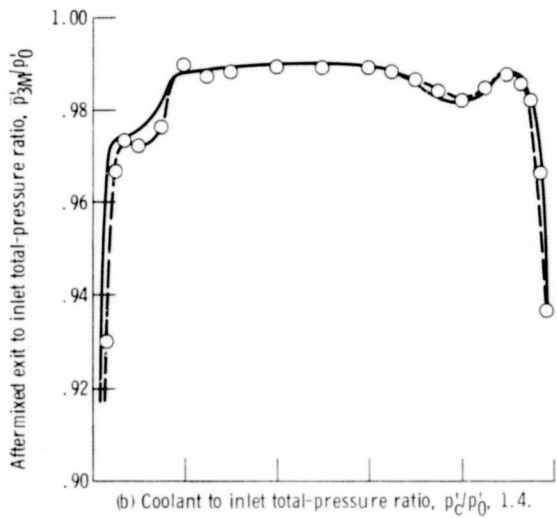
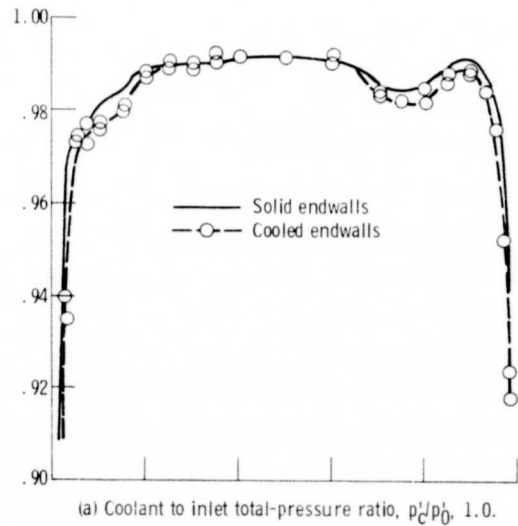
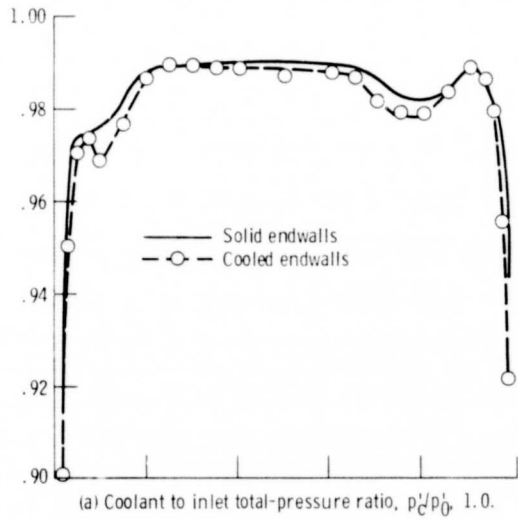


Figure 14. - Vane exit aftermixed total pressure as function of radial position for endwall coolant injected in line with inviscid streamlines.

Figure 15. - Vane exit aftermixed total pressure as function of radial position for endwall coolant injected at  $15^\circ$  to inviscid streamlines and oriented toward pressure surface.



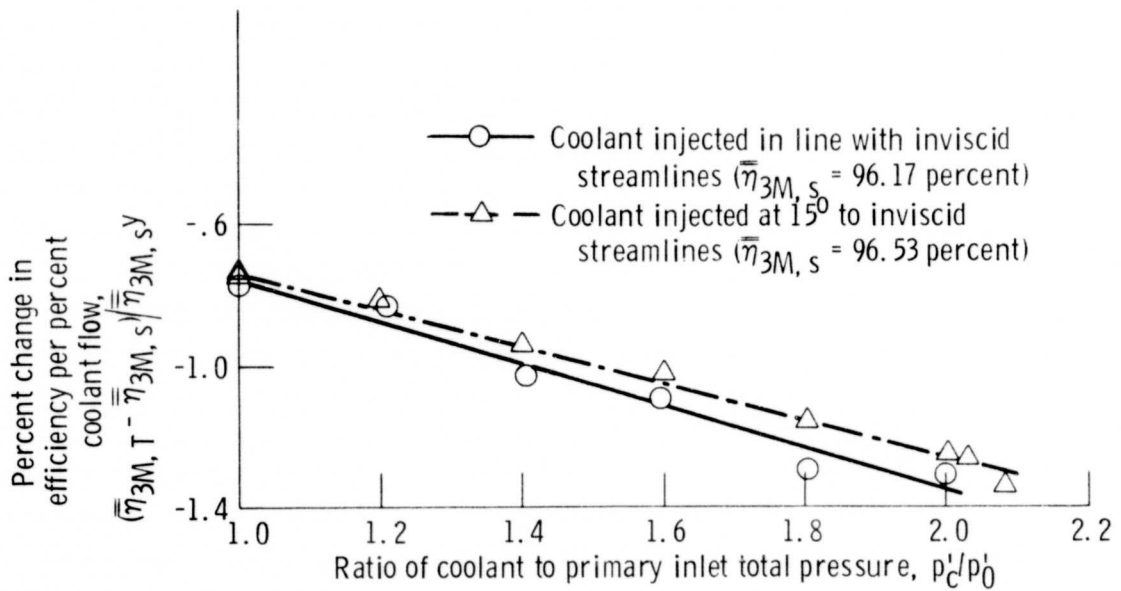


Figure 16. - Overall vane aftermixed efficiency characteristics as function of coolant to primary inlet total-pressure ratio for two cooled-endwall configurations.

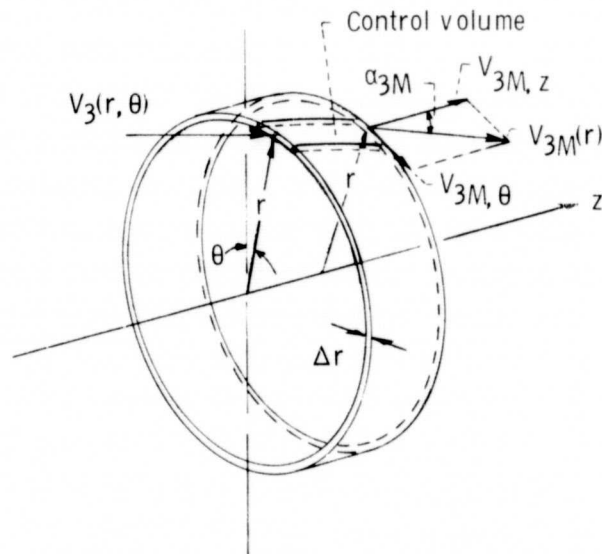


Figure 17. - Control volume for determination of aftermixed conditions (station 3M).